N 69 21114

NASA CR 66734 2

60 ap

BOEING

FILE COPY

LUNAR ORBITER PHOTO SITE ACCURACY

ANALYSIS PHOTO SITE ANALYSIS

(D2-100814-1)

SEATTLE, WASHINGTON

NASA CR-66734-1

LUNAR ORBITER PHOTO SITE ACCURACY

ANALYSIS PHOTO SITE ANALYSIS

(D2-100814-1)

By T. J. Hansen

Distribution of this report is provided in the interest of information exchange. Responsibility for the contents resides in the author or organization that prepared it.

Prepared under Contract No. NAS1-7954 by
THE BOEING COMPANY
Seattle, Wash.

for

NATIONAL AERONAUTICS AND SPACE ADMINISTRATION

REV LTR A

THE BOEING COMPANY

CODE IDENT. NO. 81205

NUMBER D2-100814-1

TITLE: Lunar Orbiter Photo Site Accuracy Analysis - Final Report - Photo Site Analysis

ORIGINAL RELEASE DATE_____. FOR THE RELEASE DATE OF SUBSEQUENT REVISIONS, SEE THE REVISIONS SHEET. FOR LIMITATIONS IMPOSED ON THE DISTRIBUTION AND USE OF INFORMATION CONTAINED IN THIS DOCUMENT, SEE THE LIMITATIONS SHEET.

MODEL ________ CONTRACT NAS 1-7954

ISSUE NO. ________ ISSUED TO: ________

PREPARED BY T. J. Hansen 10/22/68
T. J. Hansen

SUPERVISED BY W. R. Burr 10/22/68
W. R. Burr

APPROVED BY L. B. Eldrenkamp 10/23/68
L. B. Eldrenkamp

APPROVED BY J. C. Graves 10/24/68
J. C. Graves

U3 4802 1430 REV 10/67

ACTIVE SHEET RECORD

SHEET NUMBER	REV LTR	ADDED SHEETS: SHEET NUMBER	REV LTR	ADDED SHEETS: SHEET NUMBER	REV LTR	SHEET NUMBER	REV LTR	ADDED SHEETS: SHEET NUMBER	REV LTR	ADDED SHEETS: SHEET NUMBER	REV LTR
i		13a	A			26	A				
ii		13b	A			27	A				
iii		13c	A			28					
iv		36a	A			29					
v		37a	A			30	A				
vi	A	37b	A			31					
vii	A	37c	A			32	A				
viii	A	37d	A			33					
1		38a	A			34					
2		38b	A			35					
3						36	A				
4						37	A				
5						38	A				
6	A					39	A				
7	A					40	A				
8	A					41	A				
9	A					42	A				
10	A					43	A				
11	A										
12	A										
13	A										
14	A										
15	A										
16	A										
17											
18											
19	A										
20											
21											
22											
23											
24											
25											

REVISIONS

LTR	DESCRIPTION	DATE	APPROVAL
A	Revision A is the first version of this document to be released. Pages 6, 7, 8, 9, 10, 11, 12, 13, 14, 15, 16, 19, 26, 27, 30, 32, 36, 37, 38, 39, 40, 41 42 and 43 were revised and pages 13a, 13b, 13c, 36a, 37a, 37b, 37c, 37d, 38a and 38b were added in accord with comments received from NASA Research Center. The revisions are for correction and clarification.		W.R. Burr 2/5/69 Supervised by: W. R. Burr L B Eldrenkamp 2/5/69 Approved by: L. B. Eldrenkamp 2/5/69 J. C. Graves Program Manager

LIMITATIONS

DDC DOES NOT APPLY

This document is controlled by 2-5987

All revisions to this document shall be approved by the above noted organization prior to release.

PHOTO SITE ACCURACY ANALYSIS FINAL REPORT DOCUMENTS

TASK A - Photo Support Data

D2-100814-1 - Lunar Orbiter Photo Site Accuracy Analysis - Final Report - Photo Site Analysis

D2-100814-2 - Lunar Orbiter Photo Site Accuracy Analysis - Final Report - Supporting Data

D2-100814-3 - Lunar Orbiter Photo Site Accuracy Analysis - Final Report - Error Analysis

D2-100815-1 - Lunar Orbiter Improved Photo Supporting Data - Final Report - Lunar Orbiter I

D2-100815-2 - Lunar Orbiter Improved Photo Support Data - Final Report - Lunar Orbiter II

D2-100815-3 - Lunar Orbiter Improved Photo Supporting Data - Final Report - Lunar Orbiter III

D2-100815-4 - Lunar Orbiter Improved Photo Supporting Data - Final Report - Lunar Orbiter IV

D2-100815-5 - Lunar Orbiter Improved Photo Supporting Data - Final Report - Lunar Orbiter V

D2-100816-1 - Lunar Orbiter Simple Moon Residuals - Final Report

TASK B - Residual Feedback Study

D2-100818-1 - Application of Residual Feedback to Lunar Orbiter Residual Analysis - Final Report

TASK C - Tracking Data Residuals

D2-100817-1 - Lunar Orbiter Doppler Residual Study - Final Report

USE FOR TYPEWRITTEN MATERIAL ONLY

ABSTRACT AND KEY WORDS LIST

ABSTRACT

Analyses have been performed to improve the knowledge of the selenographic location of photographs taken on the five Lunar Orbiter missions. All technical areas affecting the computation of photo site locations have been re-examined, including spacecraft performance, orbit determination and the celestial environment. A checkpoint location technique was developed to measure consistency and accuracy of the results. As a result, the prime site photo location accuracy has improved from about 2.5 km to less than 1 km discrepancy. Revised attitude maneuvers, camera geometry, exposure times and state vectors were produced with improved techniques and used to generate a new set of Lunar Orbiter photo location documents.

KEY WORDS

Lunar Orbiter

Photo Site

Orbit Determination

Attitude Maneuvers

Selenographic

USE FOR TYPEWRITTEN MATERIAL ONLY

TABLE OF CONTENTS

TABLE OF CONTENTS (Continued)

USE FOR TYPEWRITTEN MATERIAL ONLY

1.0 INTRODUCTION

The purpose of this document is to report the work accomplished under Task A of the Lunar Orbiter Photo Site Accuracy Analysis, Contract NAS 1-7954. It contains a discussion of each phase of the analysis, a description of the production techniques, and summarized results.

1.1 SCOPE

The entire final report is organized within eleven documents under the three tasks A, B and C identified in the contract by the titles:

Task A - Photo Support Data

Task B - Residual Feedback Study

Task C - Tracking Data Residuals.

The documentation follows the numbering system on page v.

1.2 BACKGROUND

The purpose of the Lunar Orbiter Photo Site Accuracy Analysis contract, Task A, Photo Support Data, was to determine photo locations to greater accuracy than before possible. Work began in October, 1967, under the basic Lunar Orbiter contract (NAS 1-3800) and continued under the present contract upon closing out of the basic contract in March, 1968.

Photo support data had been generated after each Lunar Orbiter flight to define the location of each picture taken during the flight. The data presently appear in a set of five final reports as Volume VII, "Post Mission Photo Supporting Data." Each volume defines a consistent set of photo locations, but when coverage from different missions at the same area is compared, the location of any individual feature in the overlap area is often observed to be significantly different for different missions. For the prime-site photography, these discrepancies were typically about 5 km.

In addition to the discrepancies noted in the post mission photo supporting data, discrepancies had been observed during the flights upon early readout of the pictures, when corners were plotted on lunar maps. It was found that the corner locations were regularly downstream, or along-track, of the predicted locations. The post-flight calculation of the corners also verified this conclusion. In fact, an empirical three-second bias to the photo timing was used on the last flight, which successfully anticipated this error to a large extent. No explanation was found for the phenomenon during the flights.

1.3 METHOD

The method employed in generating any given unit of photo support data is shown in schematic form in Figure 1. The diagram indicates the relationship of three general areas of analysis to the final result (photo support data). These general areas are (1) spacecraft hardware data, (2) orbit determination, and (3) celestial environment, or "universe".

The approach taken in all of these areas was to examine the available data in great enough detail to reveal sources of the discrepancies, and where possible, to re-process the data with improved procedures to obtain more accurate photo locations.

1.4 RESULTS

Average photo location discrepancies have been reduced from about 2.5 km to less than 1 km for the prime-site photographs. This improvement arises largely from more accurate orbit determination. (Figure 2 lists the improvement at each point investigated). A revised set of data for all photos has been generated to replace the old Volume VII set. They are D2-100815-1 through -5, dash number indicating mission number.

2.0 CHECKPOINT TECHNIQUE

A method was devised to evaluate the consistency and accuracy of the photo locations. It was based on the use of measurements from photos as a separate data type. Photos of a common feature, or "checkpoint", were obtained from several Lunar Orbiter missions and the X, Y locations of the feature in the photos were measured. These measurements were used together with other inputs (state vector, attitude maneuvers, camera-on time) to calculate the checkpoint location for each mission. This was done in eight separate areas across the front face of the moon. The closeness of the checkpoint grouping in each area and over all areas was the criterion for judging the procedures used to generate photo support data.

Figure 3 shows the coverage by certain photo frames from three missions in a typical checkpoint area. The checkpoint appears within the small region of common overlap, and its approximate position in each frame can be seen. This area and all other areas examined for checkpoint consistency are illustrated on the moon's visible disk in Figure 4, labeled by letters "A" through "I". The approximate locations of the areas and the photo frames used for checkpoint analysis are tabulated in Figure 5.

The checkpoint areas and photo frames were selected with the purpose of obtaining the maximum number of cases of best quality (i.e., low altitude, near vertical, telephoto, three-mission coverage of the checkpoint). This insured that no one error source would be overpowering with respect to the others. An example of possible problems thus avoided is in the case of Mission IV, which was not used for checkpoint analysis because its high altitude magnifies measurement and attitude errors to an unacceptably high degree. Mission I was excluded, also, because the telephoto pictures were unusable. See Figure 6 for an illustration of typical checkpoint location errors resulting from various error sources.

Measurement of the checkpoints' positions on the photos was made in an X, Y coordinate system located at the lower lefthand corner of the photo. The photo was oriented with edge data along the left side, thus X measurements were perpendicular to the edge data and Y measurements were parallel to the edge data. Measurements were finally scaled to the frame inside dimensions, resulting in equivalent distances in millimeters on the spacecraft film.

Certain techniques were employed to maximize the measurement accuracy. The principal one was to use the reseau network found on all pictures except Mission I. The reseau marks were calibrated before each mission and have a precise X- relationship to the frame. Accordingly, measurements were small, being indexed to the nearest reseau mark; and the long distances between the index reseau marks were obtained simply by counting the intervals. Whenever a measurement was made, a measurement was also made of the local reseau interval and a proportion was obtained by dividing the measured interval into the measured distance. The sum of the proportion from the X, Y origin to the first index reseau, plus the number of reseau intervals between indixes, plus the proportion from the last index reseau to the checkpoint, multiplied by the calibrated reseau interval, yields the desired result. Figure 7 illustrates this method of measurement.

2.0 CHECKPOINT TECHNIQUE (Continued)

Use of the reseau pattern made it possible to avoid errors arising from mismatch between framelets during re-assembly. No measurements were made across framelet boundaries, eliminating y errors; and since the reseau pattern shifts with the framelet in the x direction, x errors were also eliminated thereby. In addition, negative and print non-linearities were avoided by restricting the measurements to small values in the local region of the index reseaux.

The results achieved in improving consistency and accuracy of the data are illustrated in Figure 8. In this figure, effect of the individual contributions in attitude maneuvers, orbit determination and lunar radius are shown by changes in the checkpoint locations at area "B". The checkpoint locations illustrated are three of the twenty-three indicated in Figure 5 which were used to judge the procedures.

3.0 SPACECRAFT HARDWARE DATA

Several aspects of the performance of the spacecraft itself were investigated to secure improved inputs for the calculation of photo locations. They were: attitude maneuvers, camera-on times, camera geometry and field of view. The improvement that was achieved was due principally to the maneuver angle improvement, reducing errors by about 0.4 km on the lunar surface for prime site photography. A discussion of each of the analyses is contained in the following paragraphs.

3.1 ATTITUDE MANEUVER ANGLES

The spacecraft's angular orientation for each of the exposures was previously assumed to be the designed orientation,in computing the old Volume VII photo support data. The use made of flight telemetry had been to verify that the commanded rotations had occurred in each axis, and to monitor position in the dead-band for the purpose of anticipating errors at camera-on time and applying "windage". Thus, with few exceptions, the attitude maneuver inputs were identical to the designed values appearing in the final command conference forms.

To improve the attitude maneuver data, a telemetry-analysis technique was employed which can be briefly described as "integration", in the sense of frequent adjustments over successive time intervals.

A computer program was developed which operates on the telemetered rates and positions from the Inertial Reference Unit and from the Canopus and Sun sensors. Using known attitude control system characteristics, e.g., angular acceleration levels, and keyed to readily discernible events, e.g., maneuver start points where gyro mode switching occurs, spacecraft rotation is described as a series of body axis oriented rotations. These ordered rotations cover the span from alignment with celestial references to photo time. They are determined with full account of gyro rate integrate mode drift and positions in attitude deadzones, and are adjusted for cross-coupling during maneuvers. The corrections for the effects of gyro non-orthogonality-coupling (because of gyro and body axis misalginment due to limit cycling) and inertial or geometric coupling (due to rates about other than the maneuver axes). The series of maneuvers thus determined is finally converted to three equivalent body rotations, a yaw-roll-yaw sequence which is the input to photo support data.

Accuracy of this method of handling attitude maneuvers was checked by making use of the procedure generally followed in flight, of rotating the spacecraft back as closely as possible to the original orientation (defined by Sun-Canopus lock) and then obtaining pitch and yaw readings from the Canopus sensor output. In the absence of errors in the analysis, the final equivalent three-axis maneuver should result in pitch and yaw positions exactly equal to the flight readings. The checks that were made showed accuracy at time of return to cruise orientation better than 0.2°, indicating accuracies at camera-on time typically 0.1° or less. This compares with about 0.5° typical errors previously.

3.1 ATTITUDE MANEUVER ANGLES (Continued)

A list of the attitude maneuvers for all exposures is given in D2-100814-2 of the final report, "Supporting Data."

3.2 CAMERA-ON TIMES

The spacecraft clock times associated with the exposures were carefully checked by re-reading the digital lamp time code on the GRE (Ground Reconstruction Equipment) framelet adjacent to the film and converting to decimal clock times. In the case of photo sequences, two or more frame times were checked. In the case where the time code was not read out, an estimated time was assigned based on the predicted time. These frames are presented in the table below:

L/O	Frames
I	115
II	-
III	33-36, 37, 38, 39, 40-43, 44-51, 72, 73, 74-77
IV	19, 21
V	-

For most photo sequences, it was possible to improve the relative accuracy by curve-fitting through the lamp code times. This is because the time code resolution was 0.1 seconds; since the frame interval for most sequences was only about two seconds, alterations of 0.1 seconds or less could be made which resulted in noticeable improvement relative to the neighboring frames in the sequence. A second-order least-square fit through the times was thus obtained. A sample of the results of smoothing is seen in Figure 9. The identification of every smoothed sequence is listed in Figure 10.

The link between spacecraft clock time, as indicated by the lamp code exposed on the film, and times of the telephoto and wide-angle exposures, was also re-examined, on the basis of the photographic subsystem design (see Reference 1 and 2).

As a result, telephoto camera-on times are nominally 0.09 seconds earlier than the old Volume VII set indicates. The time between telephoto and wide-angle exposures is 0.12 seconds.

A complete list of the camera-on times for all telephoto wide-angle exposures for all missions is included in D2-100814-2 of the final report, "Supporting Data."

3.3 CAMERA GEOMETRY

Geometry of the camera's field of view was analyzed by measuring the position of the telephoto corners located in the same wide angle picture. The results were reduced to data describing the angular difference between the directions of the two axes and their orientations about the axes. This analysis covered Lunar Orbiter spacecraft for missions II, III and V. Lunar Orbiter I was not done because the telephoto pictures were unusable, and Lunar Orbiter IV was not done because the wide angle corners were not visible, being in deep space for the most part. Telephoto film platen motion was considered in the analysis because the time difference between frames results in slightly different frame positions.

Final results were assumed to modify only the wide angle field of view, since the telephoto system was installed to the closer tolerances. Thus, the telephoto axis is described by the nominal values and the wide angle axis is described by adding the computed differences to the telephoto values. Figure 11 presents a table showing the difference (wide-angle - telephoto) for the three quantities; cone angle of axis, clock angle of axis, and frame orientation about the axis. The wide angle inputs to photo support data calculation are listed in D2-100814-2 of the final report, "Supporting Data." Note that frame orientation difference for EVAL inputs was assumed zero.

4.0 ORBIT DETERMINATION

The process of orbit determination (OD) requires a combination of many complex operations such as tracking data editing, least squares minimizing, trajectory prediction, and the like. The techniques used in these operations to obtain an OD solution are called the "procedures." The procedures are used in the operation of the computer program ODPL, which was supplied for the Lunar Orbiter project by JPL and which was modified both before and during the flights. Certain OD procedures were mastered during flight experience, and these formed the basis from which to start the procedures investigation for photo location improvement. A list of the flight procedures is given in Figure 12.

It was determined early that OD errors were the main contribution to prime-site photo location discrepancies. This is shown by example in Figure 13, where two different sets of harmonics tailored in obtaining an OD solution produce results about 4 km apart. (Other cases, without tailoring harmonics, showed even more sensitivity to the particular choice of procedures). Therefore, a careful search was made for an improved set of procedures which would ensure greater accuracy. As a result of this search, it was possible to improve photo site consistency by about 1 km due to OD improvements alone.

Sections 4.1 and 4.2 below, summarize the portion of the investigation done in the earlier stages of the contract, for which a more complete report is given in Reference 4. Sections 4.3 and on deal with the work done since that portion was completed.

4.1 STANDARD PROCEDURES INVESTIGATION

The initial stages of the improvement effort were directed toward an analysis of the procedures already found usable based on flight experience, especially Lunar Orbiter V. In particular, variations in the following items were tested with respect to their effects on the consistency of the photo support data:

Item	Range of Values	
Data arc length	4, 6, 10, 12, 15 hours	
Gravity model	1. LRC 4/17/66	6. LRC 10/24/66
	2. LRC 9/4/66	7. Spherical
	3. LRC 7/28B	8. LRC 11/11/66
	4. LRC 7/28A	9. LRC 10/4/67
	5. TBC S-5	10. LRC 9/30/67
Solution for harmonics	Basic model = LRC 7/28B	
Exclusion of data	14-18 minutes centered at perilune, Mission III	

4.1 STANDARD PROCEDURES INVESTIGATION (Continued)

Item	Range of Values	
Mission/Area combinations	Mission	Area
	II	C, D, F
	III	B, C, D, H, F
	V	B, D, H

A tabulation of the specific combinations tested is given in Figure 14.

An illustration of the improvement attained by using a selected combination of procedures is given below, where "discrepancy" is defined as the largest distance observed between checkpoint locations.

Area	Discrepancy, km Nominal	Discrepancy, km Improved
B	6.6	2.8
D	5.4	4.2

The combination of procedures which produced this improvement is as follows:

Data arc	10 hours, starting 1 hour before camera-on time
Gravity model	LRC 7/28B

Harmonics not in solution vector

No tracking data excluded on the basis of residual oscillations

Standard Procedures Conclusion

The investigation showed that some improvement was possible in certain lunar areas using selected procedures. Since the selected procedures did not reduce discrepancies to the neighborhood of 2 km, however, further work was directed toward improving the accuracy of orbit determination, as described below.

4.2 SHORT ARC PROCEDURES INVESTIGATION

A deviation to the standard OD technique was investigated in an attempt to provide a backup method and to gain insight into short-arc solutions. The method tested is called the "weak filter."

The weak filter technique employed the concept that a short data arc surrounding camera-on time will result in a more realistic orbit determination in the

4.2 SHORT ARC PROCEDURES INVESTIGATION (Continued)

vicinity of camera-on time. The short arc will better represent local conditions as opposed to fitting a long multi-orbit data arc that tends to average the perturbations along the orbit.

Short arc solutions are a problem for areas of one-station viewing due to a lack of sufficient tracking data for rapid convergence. The weak filter procedure used the a-priori covariance matrix to direct the final short arc solution but eliminated the constraint imposed by the a-priori state vector in standard OD procedures. Information in the covariance matrix was built up by two different methods in this study in order to compare the accuracy and consistency of the solution and also the operational characteristics.

A minor change to ODPL was required to install two weak filter options.

Method I - Short Arcs Prior to Photo Site

The first weak filter method was initiated by fitting a short data arc with two-station view as late as possible before camera-on time. Subsequent short data arcs were solved by epoch forwarding about an orbit at a time until the data arc surrounding camera-on time was reached. The covariance matrix from each solution was mapped forward and scaled (if required) to provide a-priori information to help hold together the solution from the new data. The amount of scaling of the covariance matrix was one of the critical parameters in this study, as it was necessary to retain enough information to influence the next solution but not so much as to dominate or distort it. Too much information also slows the rate of convergence.

Method II - Long Arc Prior to Photo Site

The other version of the weak filter procedure used a long data arc (10 hours) just prior to the photo site to generate a covariance matrix that was mapped forward to epoch of the short data arc surrounding camera-on time. This a-priori covariance matrix aided the final short arc solution but again, normally required scaling to reduce the influence from the previous information.

Short arc solutions using the weak filter for a variety of tests were run in search of a common technique giving consistent checkpoint locations. The variables were as shown in the table below:

Item	Range of Values
Data arc length	60, 75, 90 minutes
Previous data arcs	Successive 1-hour arcs, previous 10-hour arc
Epoch placement	0, 10 minute change
Doppler bias solution	with, without

4.2 SHORT ARC PROCEDURES INVESTIGATION (Continued)

Item	Range of Values
Model	TBC S-5, LRC 7/28B
Mission	Lunar Orbiter III, II, V
Area	C, D
Number of stations viewing	1, 2
Scaling of cov. matrix	x 1 to x 256 as required

The specific combinations tested are shown in Figure 14.

Short Arc Procedures - Conclusion

Results of the tests, discussed in some detail in Reference 4, showed that consistent solutions were not attainable via short data arcs with either version of the weak filter (I or II). Work was thus directed toward the evaluation of the residual feedback, or Kalman filter, which was incorporated into ODPL as part of Task B. A discussion of this work is contained in the following paragraphs.

4.3 EPHEMERIS TIME - UNIVERSAL TIME CORRECTION

Through frequent analysis of OD results and separate checks by NASA/MSC, it was found that an inconsistency existed in the usage of DUT (or ETUT, ephemeris time minus universal time) in various ODPL links. The evidence came partly from the experience in flight noted in section 1.0 (downtrack prediction error), and partly from the checkpoint analysis carried out in the present work. As illustrated in Figure 15, the checkpoints were invariably being located too far back in their motion--at least from a consistency standpoint. This characteristic was noted in five different areas. Upon closer examination, an irregularity in ODPL was detected and repaired. The error had been causing no more than 1.5 seconds discrepancy, depending on the mission. When repaired, the new checkpoint locations moved mostly, but not entirely, downtrack; and improved the consistency. The reason the effect was not entirely downtrack is that the timing change implied, in addition, a geometry change, which affects station doppler prediction. This alteration to the program provided the greatest overall benefit in grouping checkpoints, compared to the other techniques investigated.

4.4 RESIDUAL FEEDBACK

A separate job, Task B, was the development of a residual feedback modification to ODPL. (A report of this task is presented in D2-100818-1 of the final report.) Though its principal use was expected to be in generating statistics, it was tried in an attempt to improve the state vector solutions.

4.4 RESIDUAL FEEDBACK (Continued)

The variables in this investigation were principally program options. As shown in Figure 16, many options were made available; so the sequences of options which best carried out the test plan were exercised, namely, (0, 3, 2, 0) and (0, 1, 2, 0). Figure 16 illustrates the tracking data used in solutions of these types.

In addition to the two sequences of options, the following variables were included in the analysis:

Item	Range of Variables
Gravity model	LRC 7/28B, TBC S-5, LRC 11/11
Short data arc length	30, 60 minutes
Missions (Area D)	II, III, V

Figure 17 shows the results of use of the two sets of options compared to the standard OD solution; there is an insignificant change.

Additional results are shown below, indicating similar results using different data arc lengths.

EFFECT OF 30 MINUTE REDUCTION IN FINAL DATA ARC

Mission	Checkpoint Location $\Delta°$ Long.	Checkpoint Location $\Delta°$ Lat.
II	0	0
III	-.008	-.004
V	-.001	+.032

Residual Feedback - Conclusion

No option or sequence of options in the residual feedback capability could be found to significantly improve the checkpoint locations.

4.5 FINAL SELECTION OF PROCEDURES

Having eliminated short arc and Kalman filter procedures from among the possibilities, but with a corrected ET-UT conversion in ODPL, the problem of improving orbit determination was again attacked from the standpoint of selection of standard type procedures.

4.5.1 Gravitational Model

The effect of solution for harmonics received the most emphasis, since lack of knowledge of gravitational model was seen to deteriorate many of the other

4.5.1 Gravitational Model (Continued)

types of solutions. (In addition, solving for harmonics had been developed as a flight technique in order to reduce size of the doppler residuals.) According, the basic model chosen was that which was derived from Lunar Orbiter tracking data taken from the same type orbit; and all the highest-order coefficients, ten in number, were solved for. Thus the basic model for the low-inclination missions, LO I, II, and III, was LRC 11/11. For the high-inclination missions LO IV and V, the LRC 7/28B was used. The most noticeable benefit from this choice was the improvement in the "problem" checkpoints, single solutions located far from the mean. See Figure 18.

It was determined that coefficients should not be solved for in LO IV runs since the high altitudes prevented effects of the coefficients from being separated, and high correlation between state and harmonics made the results questionable.

4.5.2 Data Arc

The major part of the job of choosing data arc length had been done during the flights. Normally, the arcs were of three-orbit duration for two reasons: (1) forwarding considerations, in which the amount of forwarding beyond the data arc should be no greater than the data arc itself; (2) minimum data for convergence, in which with one orbit of single-station data convergence was impossible, and with two-orbits it was not always possible. The first reason, of course, has no bearing on post-flight work. The second reason does, since it has to do with ODPL operation.

A spot-check at Area D showed a checkpoint change of less than 1 km for one-orbit reduction in arc length. See Figure 19. This amount of change is approximately equal to perturbations from other sources, but no method was suitable by which superior data arcs could be chosen in every case. Thus, the nominal data arc was chosen as part of the procedures, with the exception of III P-12, where all four passes were put on the same data arc to preserve consistency.

4.6 PRODUCTION PRODUCURES

The orbit determinations for Lunar Orbiter Photo Site Accuracy Analysis were run using the general procedures listed in Figure 20. The program, ODPL, had been changed to correct the Ephemeris Time-Universal Time conversion.

4.6.1 Input Data

The planetary ephemeris used for all production orbit determinations is designated Developmental Ephemeris 19 and was originally provided by Jet Propulsion Laboratory for the Lunar Orbiter missions.

Tracking data used in the orbit determinations was from the Lunar Orbiter Tracking Data Master Tape Library compiled under CCN 157B (NAS 1-3800) and documented in Reference 3.

4.6.1 Input Data (Continued)

Lunar gravitational potential is input as a set of spherical harmonic coefficients provided by Langley Research Center. The basic lunar harmonic models used for production are the LRC 11/11 for Mission I, II and III orbit determinations and the LRC 7/28B for Missions IV and V. See Figures 21 & 22.

High order lunar harmonics were estimated with ODPL for all missions except Lunar Orbiter IV. Ten coefficients--C32, C42, C33, C43, C44, S32, S42, S33, S43, S44, were estimated as a standard procedure. The number of estimated harmonics was reduced to eight (C44 and S44 reset to nominal values) only when the ten-harmonic estimate proved to be nonconvergent.

Epoch placement and data arc length were unchanged from the orbit determinations reported in the postmission photo support documents. All of the photo sites are included within these data arcs, with the exception of a few secondary sites. Some of the postmission orbit determinations were not repeated because the photo sites originally associated with those data arcs could be included in other solutions.

The orbit determinations used all available two-way and three-way doppler tracking data, including data taken during photo readout with 20 and 30 second doppler count time and all data surrounding perilune. The inclusion of three-way doppler dictated the requirement to estimate the value of doppler bias. This was a standard procedure even though bias is known to have been removed from most data in the tracking data master tape library.

The orbit determination solution was mapped to a time about one minute prior to each frame or series of frames within the data arc, using the modified lunar model.

An additional requirement of each production run was to generate a trajectory using the solution state vector from the orbit determination, but with a gravitational field defined by a simplified triaxial model ($J20 = 2.073 \times 10^{-4}$; $C22 = 0.203 \times 10^{-4}$) rather than the modified high order harmonic model used in the solution. Doppler residuals were then computed from this special trajectory and plots of the residuals were obtained. The residual plots are published in D2-100816-1, Lunar Orbiter Simple Moon Residuals - Final Report.

4.6.2 Program Output

The most concise form of output from orbit determination production runs is the computer generated orbit determination report. Each report includes the epoch of the data arc, selenocentric spacecraft state vector at epoch, selenographic orbital parameters corresponding to the state vector solution, and a listing of the lunar harmonic model (up to fourth order) as modified by the ODPL solution. A summary discussion and a list giving identification number, epoch, data arc length and a mapped photo sites are in each mission's "Improved Photo Supporting Data" document (D2-100815-X). The epoch reports for each mission are also included.

4.6.2 Program Output (Continued)

Additional output is from the photo site mappings in the form of orbit determination reports. The map time reports are identical in format to the epoch reports although the lunar harmonic model is not relisted. The content of these mapping reports is used as input data to the Photo Evaluation Program (EVAL). The map time report listings are published in the "Supporting Data" document D2-100814-2.

The identification numbers for the orbit determinations and the mappings are derived primarily from the photo site designations used during the Lunar Orbiter missions. The first digit indicates the mission number and the next character (A, P, S or V) indicates a primary or secondary site followed by the site number. The letters A, P, S or V are the identifiers used during the mission. During Mission I prime sites were designated by A. Mission II and III used P for prime site and S for secondary site. Mission IV is designated by orbit number. Mission V used V for photos at perilune and A for photos at apolune. Sites with no site designation during the missions, such as film set frames are identified by F. The orbit determination number is the same number as the first photo site in the data arc with the exception of Item 16 (an oversight) and Mission IV. The orbit number provided a better reference for Mission IV OD identification.

The complete printed output from all ODPL production runs, including simple moon residual plots, is recorded on microfilm for ease in storage of the data.

5.0 CELESTIAL ENVIRONMENT

A combination of mathematical models were used to express the celestial environment as it influenced the L/O trajectories and the data gathered. Where photo site locations were adversely affected by the assumptions, improvements were incorporated if possible. The principal departure from convention was in the adoption of different values of lunar radii as an input constant to the photo data program EVAL. These radii varied from 1733 to 1738 km across the Apollo region and typically affected photo corners 0.5 km or less for prime-site photography. It was not possible to simulate the recently revealed mass concentrations near the lunar surface due to the timing of this work. However, it is reasonable to expect that photo location accuracy will be markedly improved when such a gravitational model becomes available.

The following paragraphs describe the investigation of the "universe."

5.1 LUNAR EPHEMERIS

The JPL lunar ephemeris tape DE-19 was used in the production ODPL solutions. This ephemeris includes the revised Eckert corrections to Brown's theory, plus some second order terms. The integrated ephemeris was also tried, but produced insignificant differences in the doppler solutions when compared with the solutions using DE-19. The ephemeris tapes used in the published post mission data were as follows: Missions I and II "EPHEM 1", Missions III and IV DE-15, and Mission V DE-19.

5.2 MOON'S SIZE AND SHAPE

The physical dimensions of the moon were investigated based on Lunar Orbiter data from three different viewpoints: station occultations, checkpoint consistency, and angular separation between features photographed from high and low altitude. For the production photo support data, values varying from 1733 km to 1738 km were input depending on photo site location. A discussion of the analysis is given below.

5.2.1 Station Occultation

Size and shape of the moon was briefly examined in the "Occultation Study" of NAS 1-3800 (CCN 157B), confined, of course, to the visible lunar disk. A final report on this work is found in Reference 4. The results, though having considerable scatter, indicated a smaller radius than the nominal (1738 km). This agrees with Ranger impact data (Reference 5) and Lunar Orbiter V/H ratio telemetry (Reference 6).

5.2.2 Mean Radius Study

Background

Using cases like those selected for the checkpoint consistency tests, overall effect of lunar radius was examined by using lunar radius as an independent variable and monitoring the statistical grouping of checkpoints as a dependent variable.

The sketch in Figure 23 illustrates how lunar radius affects the computation of feature location. Note that the more obliquely the feature is viewed, the more sensitive is its location to lunar radius.

Results

Several different values for the mean lunar radius were used to compute the coordinates of the checkpoint features and a single value was chosen as most appropriate to the multi-mission consistency. This value, 1736 km, reduces the deviations from the mean checkpoint locations in nine of eleven areas and reduces the standard deviation by 10%.

Assumed Lunar Radius (km)	Standard Deviation, (km)
1738	1.08
1736	0.97
1734	1.19

The number of sample cases included in the calculation of the above standard deviations was 23. A later analysis, using results from the improved orbit

USE FOR TYPEWRITTEN MATERIAL ONLY

5.2.2 Mean Radius Study

determination procedures, and having 14 sample cases, shows similar results (see Figure 24).

While the reduction in sigma is significant in itself, it may be noted that the situations have nearly vertical viewing and therefore exhibit little sensitivity to variations in lunar radius. A more substantial case for a reduced moon radius is found in the high tilt angle photos of the above checkpoints, where the deviation from the mean was typically reduced 50 to 75 percent, to approximately 1.0 or 1.5 kilometers. The table below illustrates the improvement observed in these cases.

CHECKPOINT IDENTIFICATION			DEVIATION FROM THE MEAN (KM)	
Area	Frame No.	Tilt Angle	Rm = 1738	Rm = 1736
G	III-136	54°	3.1 km	1.0 km
E	I-137	41°	21. km	1.2 km
E	II-169	25°	2.1 km	1.2 km
H	III-171	56°	5.9 km	1.5 km
C	V-76	35°	1.3 km	0.7 km
F	III-161	65°	5.1 km	1.3 km

5.2.3 Site Elevation Study

A separate study was made of the local lunar radius at several areas. The principle involved here was one of triangulation; a comparison of the angular separation between two surface features, subtended at the spacecraft, seen in high altitude vs. low altitude photos. A sketch illustrating the geometry is shown in Figure 25.

Low altitude photos from Mission II and III were found which could be located in L/O IV (high altitude) telephoto pictures. Features found at or near the corners of the low-altitude wide-angle photos were measured on the L/O IV photos, then located by latitude and longitude using the program OPAL. With these surface locations, and the best known low-altitude spacecraft position, the angle between pairs of features, subtended at the low-altitude spacecraft, were computed. This angle was compared against the "known" angle as determined by measurement on the low-altitude photo. The local lunar radius was found that produced the best agreement between computed and known angles, on a least squares basis. Finally, the set of local lunar radii determined in this manner were plotted vs. longitude. See Figure 26. Since most of the prime sites were near-equatorial, the plotted site elevation represents all sites at the same longitude within the Apollo zone.

5.2.3 Site Elevation Study (Continued)

Data were also generated using features located on LAC charts instead of by Lunar Orbiter IV photo measurements; these points are separately identified on Figure 26. A comparatively large number of points were taken to avoid any local discrepancies in map-matching.

The value of lunar radius found in Figure 26 was used for input to the photo support data up to latitudes of ±10°. Outside the ±10° latitude band and the longitude range -50° to 40°, a value of 1736 km was input. A list of the lunar radii used for EVAL input is contained in D2-100814-2 of the final report, "Supporting Data."

5.3 SELENOGRAPHIC COORDINATE SYSTEM

Specification of the angular orientation of the moon is part of the job of computing photo site locations. An investigation was made to determine the presence of any significant bias in the moon's orientation, and to apply a correction if necessary. This section describes that investigation, its results, and conclusions.

The positions of the moon's equator and prime meridian are specified with respect to the true equinox of date and the true of date earth equator plane by the three Euler angles i, Ω, and Λ. The formulation of these angles are time variant, empirically determined based on observation and augmented by lunar libration theory. The nominal expression of orientation, supplied for the Lunar Orbiter software by JPL, is given in Reference 7. . Earth based observation is subject to a number of errors, some of which are (1) uncertainties in the "control" features on which the computations are based, (2) values of the librations, (3) errors in photo plate constants to correct for scale and orientation, and for removal of atmospheric effects, and (4) errors in observation due to the lunar phase effect.

Reference 8 reveals one sigma (1σ) errors in the coordinates of lunar features of 0.5 to 1.0 kilometers in latitude, and 0.4 to 2.0 kilometers in longitude over most of the front face of the moon, with errors as great as 5 to 10 kilometers for features near the limbs. Since the Euler angles i, Ω, and Λ are determined in essentially the same manner as lunar feature coordinates (see Reference 9 and 10), the determination of the Euler angles are assumed to have the same order of uncertainty.

5.3.1 Method of Investigation

Photos from the five Lunar Orbiter missions were analyzed to find a number of frames containing in common a prominent lunar feature which could be used as a checkpoint. Each feature chosen as a checkpoint had been photographed in two to five independent frames. The selenographic coordinates (latitude and longitude) of a particular feature were determined separately in each incident photo frame and the several solutions compared. The deviations from the mean location were computed as a measure of the accuracy and consistency of the photo location data.

Since the orientation of the selenographic coordinate system is time variant, it directly affects the solutions obtained for the feature identified in the different photos, because they were exposed at different times. This fact permitted an investigation of the validity of various moon orientations.

A computer program (EASE) was written which employed an iteration technique to solve for a set of perturbed Euler angles optimized to produce the most consistent checkpoint locations. Each set of photo frame data input to the program was individually processed through the photo geometry routine to determine the longitude and latitude of its checkpoint. Using the several

USE FOR TYPEWRITTEN MATERIAL ONLY

5.3.1 Method of Investigation

solutions obtained for a given checkpoint, the density of their grouping was computed in terms of mean longitude and latitude, deviations from the mean, and sum of the squares of the deviations. At this point, the nominal Euler angles were perturbed slightly and the process repeated, resulting in new values for checkpoint locations and the density of the grouping. Continued iteration resulted in a set of modified Euler angles which produced the least sum of the squares of the deviations in longitude and latitude. This technique used the assumption that the perturbation to any Euler angle remains constant over the entire period of time.

5.3.2 Results

In a few areas a modified set of Euler angles was found which resulted in some improvement in the checkpoint consistency. However, in most of these cases the amount of the improvement was negligible with respect to the overall dispersions.

The runs which contained input data for only one or two checkpoint areas generally converged in solutions leading to slight reductions in the dispersions, but the perturbations to inclination, i, varied in both sign and magnitude. When more than two checkpoint areas were included in the data, the program exhibited trouble in attaining a solution and often diverged after attempting many iterations.

5.3.3 Conclusions

The present study did not reveal any superior means of expressing the moon's orientation, thus the nominal values were used as described in Reference 7.

Any improvement made possible by perturbing the moon's orientation is negligible compared to uncertainties arising from other sources, particularly orbit determination.

It should be noted that while this investigation concludes that no sizeable biases exist in the nominal formulation of the Euler angles, the possibility of an improved definition of the selenographic coordinate system is not ruled out. Indeed, preliminary checks versus the Apollo transformation program, which is based on more recent analysis of the moon's orientation, indicates that, in general, the consistency was roughly 0.2 km better using the Apollo data. Unfortunately, it was not possible to incorporate the Apollo programming into the Lunar Orbiter software.

6.0 ERROR ANALYSIS

An error analysis was made for representative photo frames for the five missions. Selenographic latitude and longitude errors were determined for the camera axis intercept, corner points, and points approximately midway between the corners, for both the telephoto and wide-angle lenses. The associated eigenvalues, rotation angle, and correlation coefficient for each frame point were also determined for the total error. Contributions to the total error were made by navigation, attitude, camera-on time and moon radius errors.

The table on Figure 27 shows the approximate variation of sigma within the frame, in the North-South (LAT) direction and in the East-West (LONG) direction. The smaller value generally corresponds to a point in the photo closest to the spacecraft; the larger to a point farthest away. For Missions I, II, III, and V, it is seen that errors typical for Apollo frames are less than 0.4 km in latitude and longitude for the telephoto lens (T) and less than 0.6 km in latitude and longitude for the wide-angle lens (W). For some Apollo frames, larger errors are observed (a few km and more), due to a combination of factors including:

1) attitude error - due partially to large attitude maneuvers for some frames, in conjunction with increased altitude above 46 km for some frames, making the attitude error larger,

2) large camera axis tilt angle - making the error due to moon radius larger.

Generally speaking, for Missions I, II, III, and V frames at low altitude (meaning 46-240 km), the total photo error variance is a combination of significant contributions from attitude and navigation sources, with a significant contribution for some frame points due to moon radius error, especially for the W lens. For altitudes greater than approximately 240 km, the attitude error is the predominant contributor. Errors of a few km are not uncommon for Missions I, II, III, and V as indicated in the Error Analysis Summary Table.

The photo errors due to camera-on time error is essentially negligible for all frames.

Frames taken at high altitude reflect the predominant attitude errors, with an increased attitude error for Mission IV frames where the maneuver is not made relative to celestial alignment, but to the previous attitude. The Error Analysis Summary Table indicates this trend for one, three, and five attitude maneuvers.

The navigation statistics do not include the effects of uncertainty in lunar gravitational harmonics; since this is a major cause of uncertainty in many cases, the total statistics therefore suffer as a result, having unrealistically small sigma values for those cases. The amount of the deficiency is estimated to be on the order of 0.5 - 1.0 km. Inability to accurately express the moon's gravitational potential mathematically is seen to be the

6.0 ERROR ANALYSIS (Continued)

reason for the deficiency. The remainder of the navigation error sources are represented, e.g., DSN radar, earth mass, and station location. It is not apparent that gravitational model uncertainties can be expressed even when a more accurate model becomes available; but their effects on navigation statistics will hopefully be unimportant with respect to other contributions.

A more complete discussion of the navigation statistics is given in D2-100814-3 of the final report, "Error Analysis."

7.0 EVAL PROGRAM CHANGES

This section describes the modifications made to program EVAL as a part of the work to improve the photo location accuracy. The purpose of the changes was two-fold, 1) to produce more precise photo data by refining some of the simplifying assumptions made in the original analysis, and 2) to provide more useful data and greater convenience for the users.

7.1 SEPARATION OF THE CAMERA SYSTEMS

The high resolution camera and the moderate resolution camera were previously considered as having coincident geometry and shutter mechanisms. This assumption greatly reduced the programming task, but nevertheless, introduced some element of error. It was decided to correct this situation with a program change and utilize the results of the camera geometry and camera shutter time investigations (see Section 3.2 and 3.3).

The separation of the two camera systems required extensive internal program modifications while the changes to the output were limited to increased volume with relatively little format modification. The output now consists of two separate pages of photogrammetric data; one page for each camera, labeled near the top.

The camera-on times, and accordingly, the state vectors, are different for each lens system. Since the separation of the shutter times is a constant related to the internal camera hardware, the program input is shutter time for each high resolution frame and a differential time in seconds to obtain the moderate resolution shutter times.

7.2 COORDINATE SYSTEMS

In order to make the output convenient and useful to as many users as possible, the state vectors at the camera-on times are now referenced in two coordinate systems. These systems, the selenographic of date and the selenocentric 1950.0 are the two in most common usage for lunar study.

7.3 SELENOGRAPHIC COORDINATES OF THE FIDUCIALS

Program OPAL (Oblique Photo Analysis, L/O) was built into the user program EVAL as an additional link for the purpose of computing the location of the projection of frame notch points on the lunar surface. The required inputs to OPAL are the coordinates (X, Y) of the point as it appears in the photo as well as the spacecraft position vector, attitude maneuvers, etc. as used by EVAL. The measured coordinates of the fiducial marks were provided by the Camera Calibration data (Reference 11 through 14). The notch identification adopted in those reports is used in the EVAL output.

7.3 SELENOGRAPHIC COORDINATES OF THE FIDUCIALS (Continued)

The (X, Y) coordinates output alongside the notch identification are those giving the sawtooth location in a coordinate system whose origin is the center of the photo. The positive X axis is to the right and the positive Y axis is upward as one views the photo positive with the edge data to his left. This differs from the ACIC coordinates, which are indexed to the principal point of autocollimation or a geometric mean.

7.4 EPHEMERIS TO UNIVERSAL TIME CORRECTION

Routine SELGRA called by both OPAL and EVAL was modified to use an input variable for the time correction, Δt, the time difference between Ephemeris Time and Universal Time. The previous versions of SELGRA relied on a constant value for Δt that was fixed within the routine, thereby introducing a small error, since Δt changes with time. The change puts this variable into the calling sequence of SELGRA and provides the routine with the values of Δt appropriate to the camera-on time.

8.0 REFERENCES

1. L-018375-RU, "Photographic Subsystem Reference Handbook for the Lunar Orbiter Program," (Eastman-Kodak), March 15, 1968.

2. D2-100112, "Spacecraft Photo Subsystem Design Control Specification-Lunar Orbiter, " (Boeing), April 1, 1964.

3. D2-100809-1, "User's Guide To the Lunar Orbiter Tracking Data Master Tape Libraries," (Boeing), February 12, 1968.

4. D2-100813-1, "Final Progress Report CCN 157B - Lunar Orbiter Photo Site Analysis," (Boeing), April 22, 1968.

5. "Measure of the Moon," Proceedings of the Second International Conference on Selenodesy and Lunar Topography," June 4, 1966.

6. D2-100727-3, "Lunar Orbiter I Final Report, Volume III - Mission Performance."

7. TR 32-41, "Selenographic Coordinates," (JPL), February 24, 1961.

8. Icarus #7, 1967, "Absolute Coordinates of Lunar Features," G. A. Mills.

9. Physics and Astronomy of the Moon, edited by Z. Kopal, Academic Press, 1962.

10. Explanatory Supplement to the Ephemeris, H. M. S. Nautical Almanac Office, 1961.

11. Lunar Orbiter I Calibration Report, USAF (ACIC), December 1966.

12. Lunar Orbiter II Calibration Report, USAF (ACIC), March 1967.

13. Lunar Orbiter III Calibration Report, USAF (ACIC), August 1967.

14. Lunar Orbiter IV and Lunar Orbiter V Calibration Report, USAF (ACIC), January 1968.

USE FOR TYPEWRITTEN MATERIAL ONLY

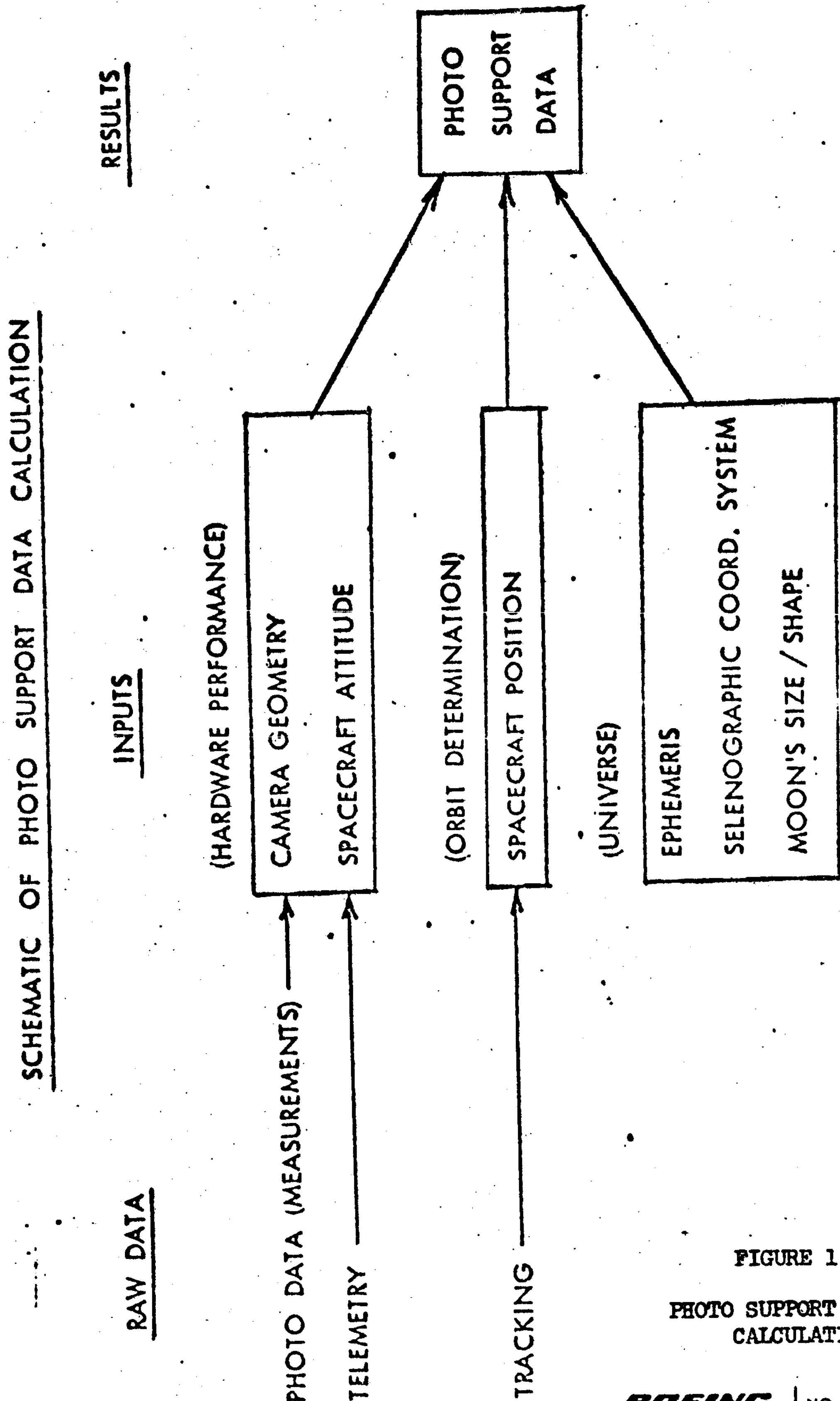

FIGURE 1

PHOTO SUPPORT DATA
CALCULATION

CHECKPOINT CONSISTENCY

MAXIMUM DISPERSION*

AREA	POST FLIGHT DATA	NEW PROCEDURES
A	11.1 KM	2.1 KM
B	5.6	2.5
C	3.5	2.0
D	5.5	2.2
F	1.6	2.1
G	8.1	2.6
H	4.7	2.0
I	5.9	2.3

* Approximately double the dispersion from mean location.

FIGURE 2

CHECKPOINT CONSISTENCY

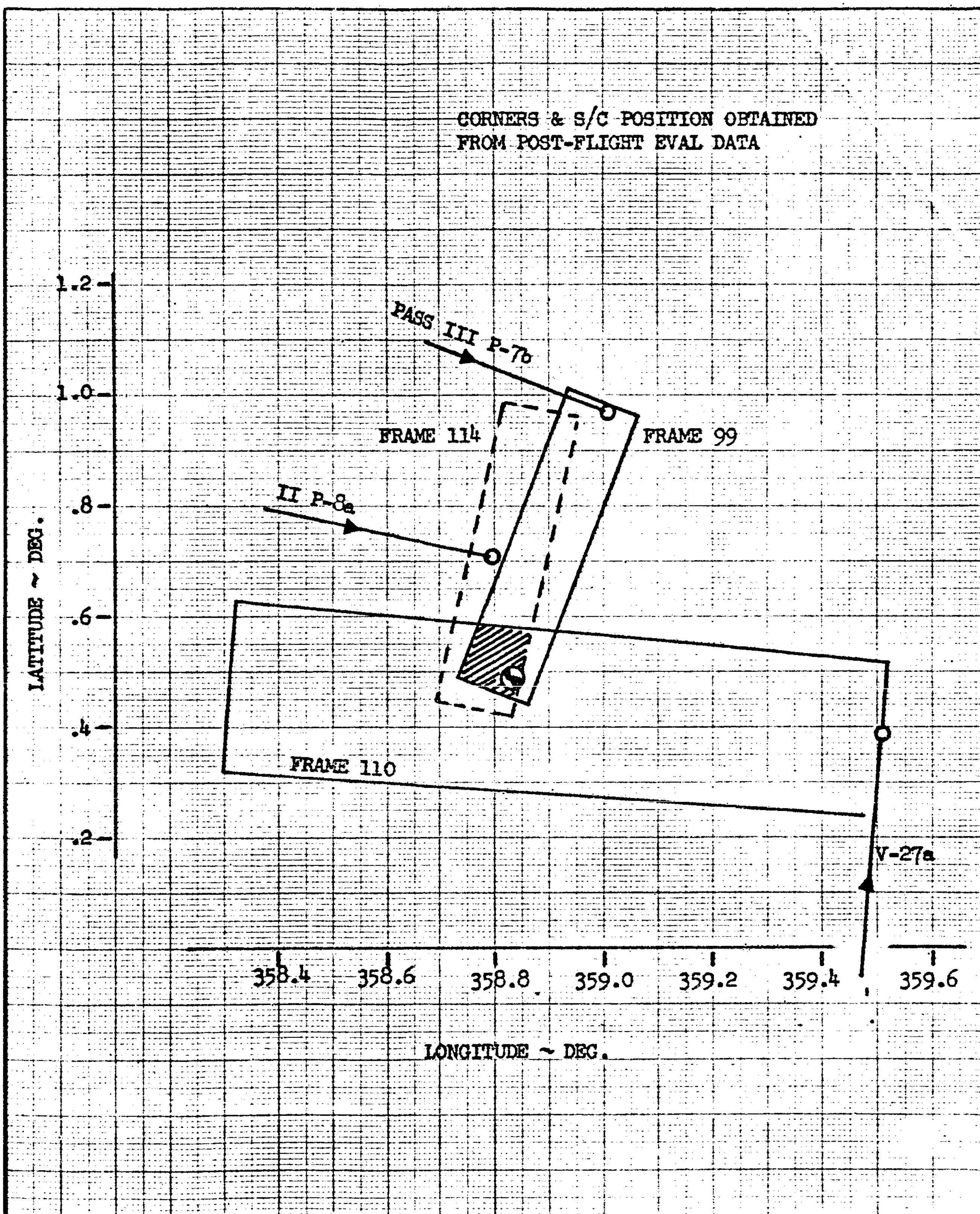

	INITIALS	DATE	REV BY INITIAL	DATE	TITLE	MODEL
CALC					COVERAGE OF AREA "D" CHECKPOINT	FIGURE 3
CHECK						
APPD.						
APPD.						

U3 4013 8000 REV. 1/66

REV LTR A

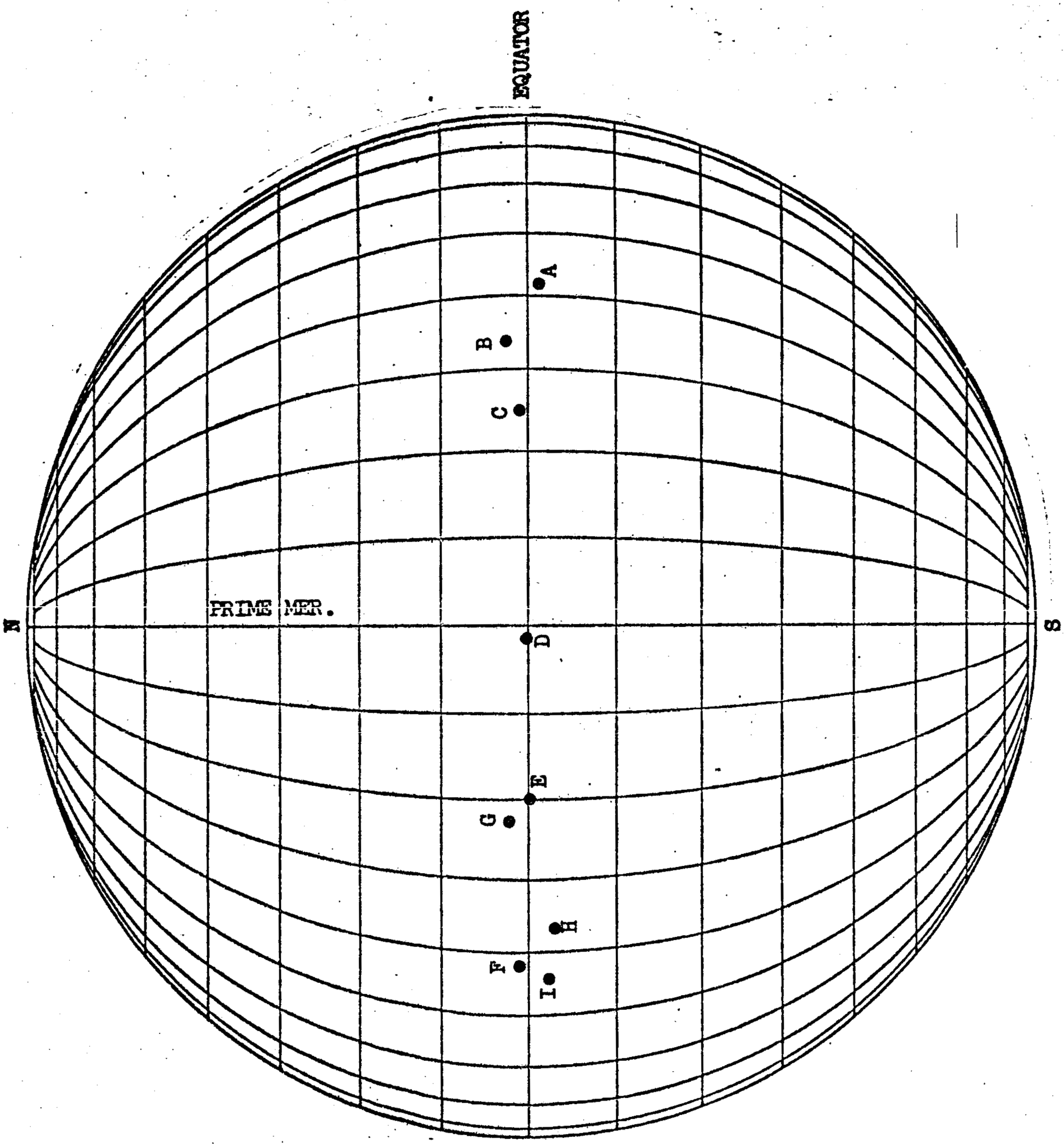

FIGURE 4

USE FOR TYPEWRITTEN MATERIAL ONLY

CHECKPOINTS MEASURED

AREA	APOLLO DESIGNATION	APPROXIMATE LOCATION Long°	Lat°	CHECKPOINT FRAMES		POSITION IN PHOTO* X, mm	Y, mm
A	IP-1	42	-1	I	66W	-26.900	- 2.215
				III	25W	18.630	-11.660
				V	45T	-24.940	109.490
B	IIP-2	34	3	II	40T	1.581	103.816
				III	6T	-12.726	-66.335
				V	57T	14.021	- 9.846
C	IIP-6	24	1	II	83W	- .195	-14.980
				II	91T	- 1.400	32.200
				III	62T	14.710	76.200
D	IIP-8	-1	0	II	114T	19.396	-72.766
				II	123T	-11.629	77.050
				III	99T	- .927	-83.691
				V	110T	-11.424	5.577
				V	114T	1.649	7.000
E	IIP-11	-20	0	I	137W	9.350	-17.110
				II	169W	-21.980	32.090
F	IIP-13	-42	1 1/2	II	198T	8.995	-100.600
				II	205T	7.970	53.700
				III	165T	21.620	- .200
G	IIIP-9	-23	-3	I	169W	-26.430	22.180
				III	142W	22.730	21.780
				III	149W	27.400	12.950
				III	159W	25.380	31.38
H	IIIP-11	-37	-3	III	180T	21.11	16.00
				V	170T	20.91	-12.10

* Origin at center of frame, scaled to actual frame size.

FIGURE 5

CHECKPOINTS

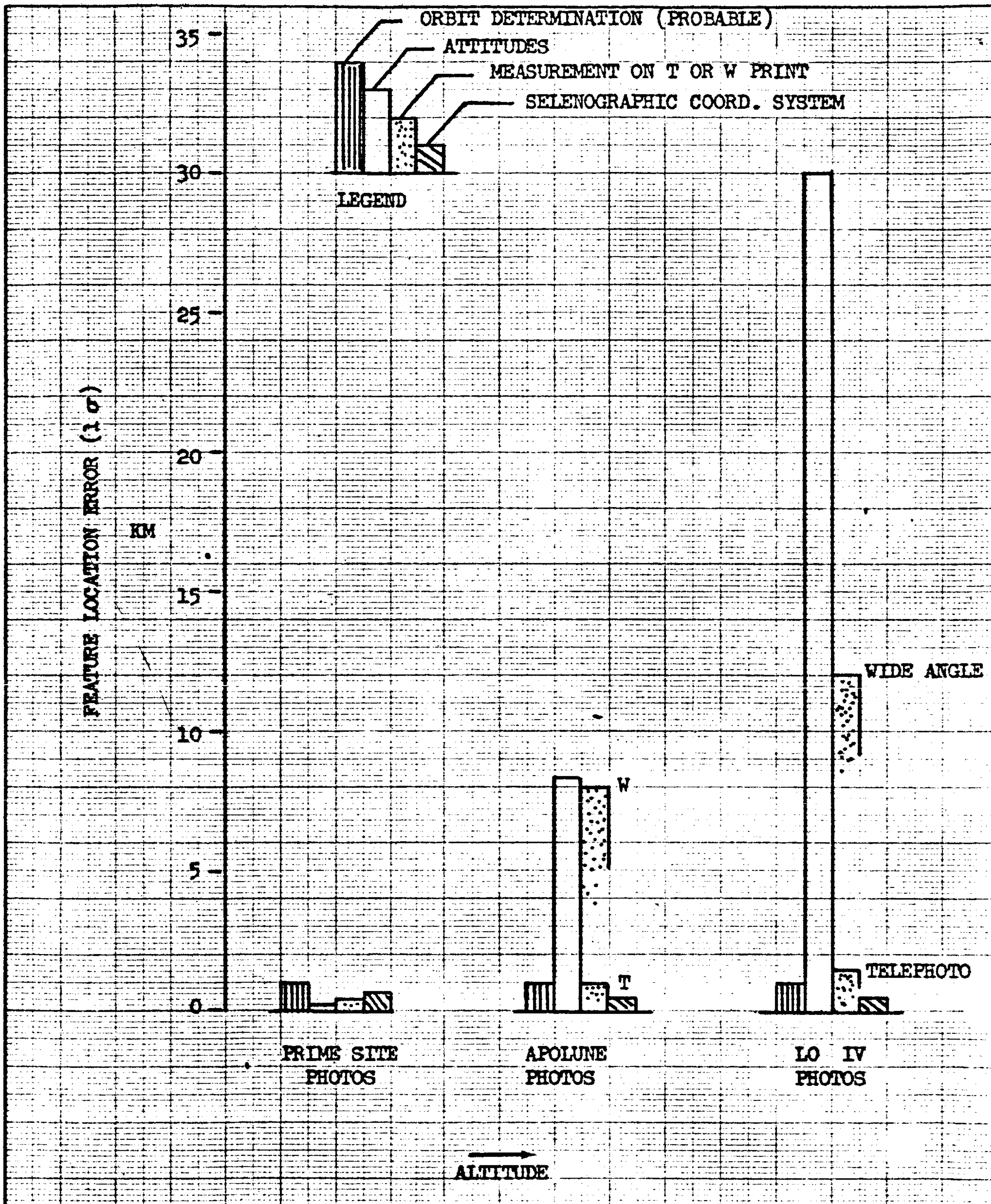

	INITIALS	DATE	REV BY INITIAL	DATE	TITLE	MODEL
CALC					TYPICAL PHOTO LOCATION ERRORS	FIGURE 6
CHECK						
APPD.						
APPD.						

U3 4013 8000 REV. 1/66

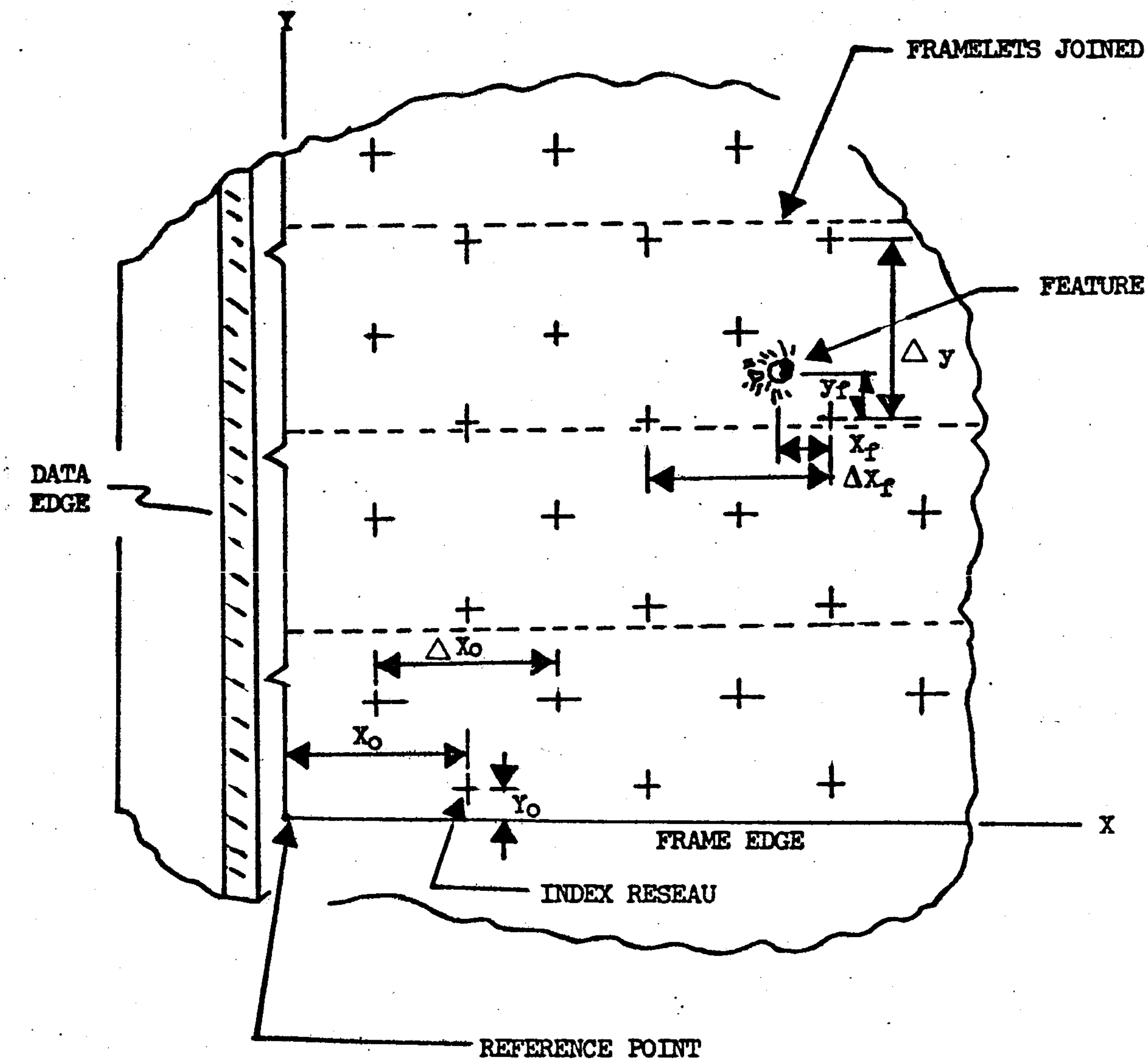

COORDINATES OF FEATURE:

$$X = \left(\frac{X_o}{\Delta X_o} + 2 + \frac{-X_f}{\Delta X_f} \right) \cdot R_x$$

$$Y = \left(\frac{Y_o}{\Delta Y} + 2 + \frac{Y_f}{\Delta y} \right) \cdot R_y$$

(Rx, Ry = calibrated reseau intervals)

METHOD OF PHOTO MEASUREMENT

FIGURE 7

U3 4802 1433 REV. 6/65
SHEET

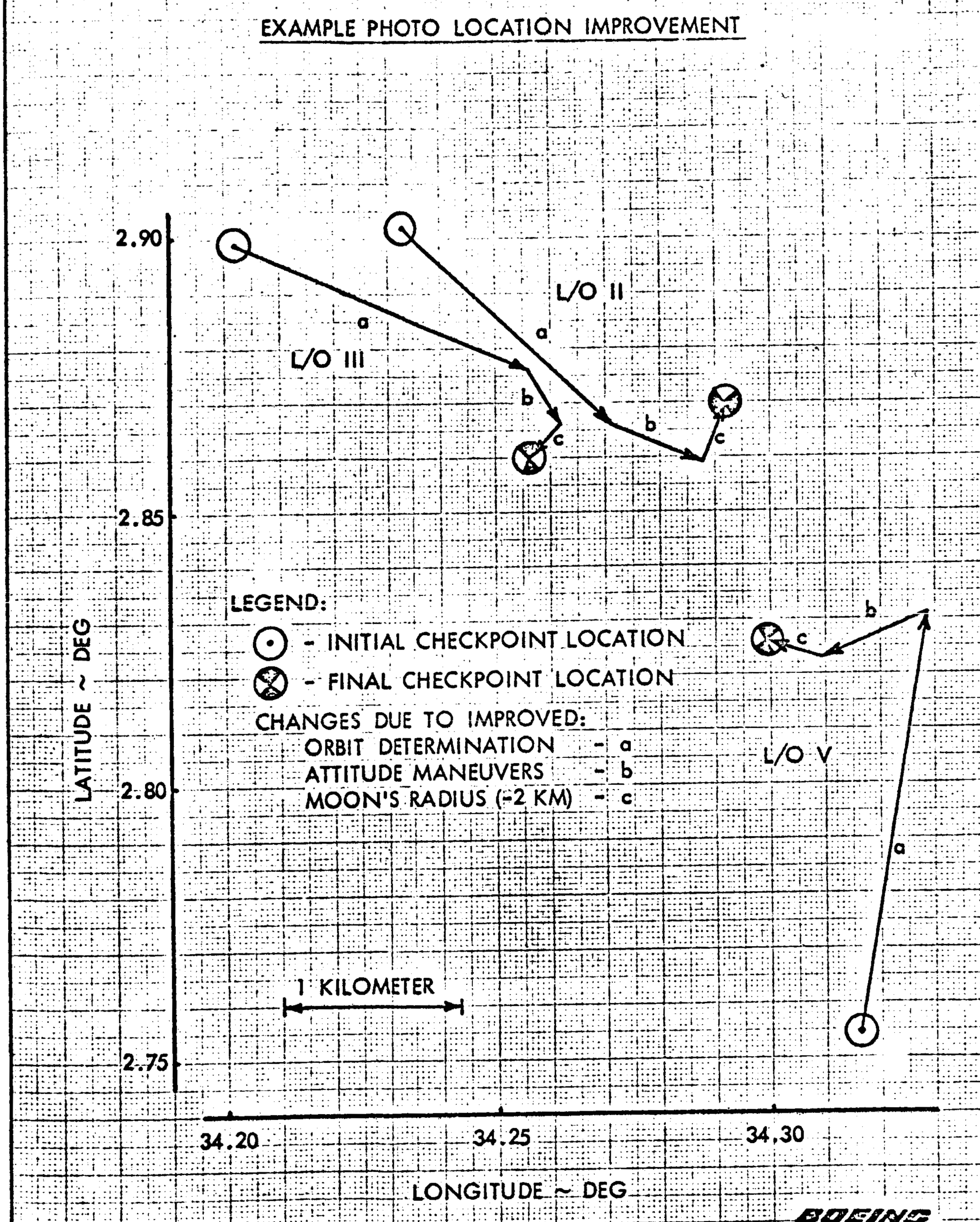

FIGURE 8

T. J. HANSEN 7/18/68

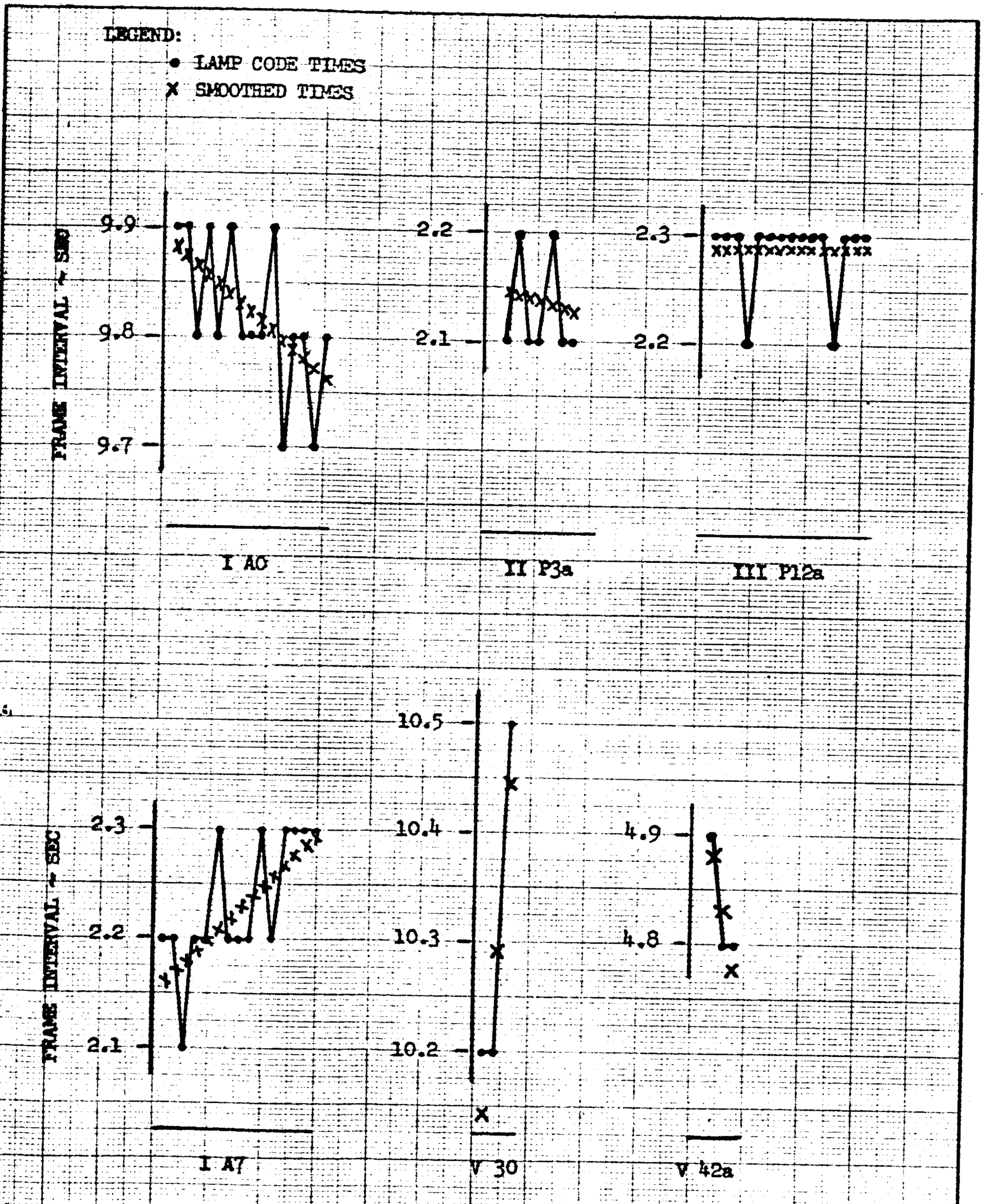

	INITIALS	DATE	REV BY INITIAL	DATE	TITLE	MODEL
CALC	TH	3/68			SMOOTHED EXPOSURE TIMES	FIGURE 9
CHECK						
APPD.						
APPD.						

U3 4013 8000 REV 1/66

CAMERA-ON TIME SEQUENCES SMOOTHED

I	II	III	V
A0	P-1	P-7a	A-1
A1	S-2a	P-7b	A-2
A2	S-2b	S-17	V-1
A3	P-2	S-19	V-8a
A4	P-3a	P-8	V-11a
A5	P-3b	P-9a	V-14
A7	P-4	P-9b	V-23.1
A8.1	P-5	P-10	V-24
A9.2a	P-6a	P-11	V-27b
A9.2b	P-6b	P-12a	V-28
	P-7a	P-12b.1	V-29
	P-7b	P-12c	V-30
	P-8a		V-31
	P-8b		V-32
	P-8c		V-35
	P-9		V-36
	P-10a		V-37
	P-10b		V-40
	P-11a		V-42a
	P-11b		V-42b
	P-12a		V-45.1
	P-12b		V-46
	P-13a		V-48
			V-49
			V-50
			V-51

FIGURE 10

USE FOR TYPEWRITTEN MATERIAL ONLY

WIDE ANGLE GEOMETRY

WITH RESPECT TO TELEPHOTO

MISSION	CAMERA AXIS CONE deg.	CAMERA AXIS CLOCK deg.	FRAME ORIENTATION* deg.	FRAME ORIENTATION σ
I	0	0	0	-
II	-.027	.122	-.007	.099
III	.090	.059	-.028	.065
IV	0	0	0	-
V	-.024	.148	-.107	.092

* Zeros were input for frame orientation for EVAL input.

FIGURE 11

PROCEDURES DEVELOPED

- LUNAR MODELS
  - L/O II - LRC 9/4 (BASED ON L/O I TRACKING)
  - L/O III - TBC C-2 (SIMPLE CONTROL MODEL BASED ON MODIFIED L/O II ORBIT)
    - LRC 11/11 (BASED ON L/O I TRACKING)
  - L/O IV - LRC 11/11
  - L/O V - TBC S-5 (SIMPLE CONTROL MODEL BASED ON MODIFIED L/O IV ORBIT)
    - LRC 7/28 B (BASED ON L/O III AND L/O IV TRACKING - TESTED BY TBC PRIOR TO MISSION V)
- SOLVE FOR LIST
  - L/O II, III, V - STATE VECTOR PLUS 10 HIGH ORDER HARMONICS (TAILORING)
  - L/O IV - STATE VECTOR ONLY
- PERILUNE DATA
  - L/O II - DELETED
  - L/O III, IV, V - INCLUDED, SINCE IT APPEARED TO BE REAL DATA
- DATA ARC LENGTH
  - L/O II, III, IV, V - ≅ 12 HOUR ARC USED
- TRUE ANOMALY AT EPOCH
  - L/O II, III IV, V - NEAR ($\pm$ 30°) BUT NOT AT APOLUNE
- STATE VECTOR FORWARDING
  - L/O II - 9/4 "TAILORED" FOR EPOCH, 9/4 FOR CAMERA-ON-TIME (COT)
  - L/O III - 11/11 "TAILORED FOR EPOCH AND COT
  - L/O IV - 11/11 FOR EPOCH AND COT
  - L/O V - 7/28B "TAILORED" FOR EPOCH AND COT

FIGURE 12

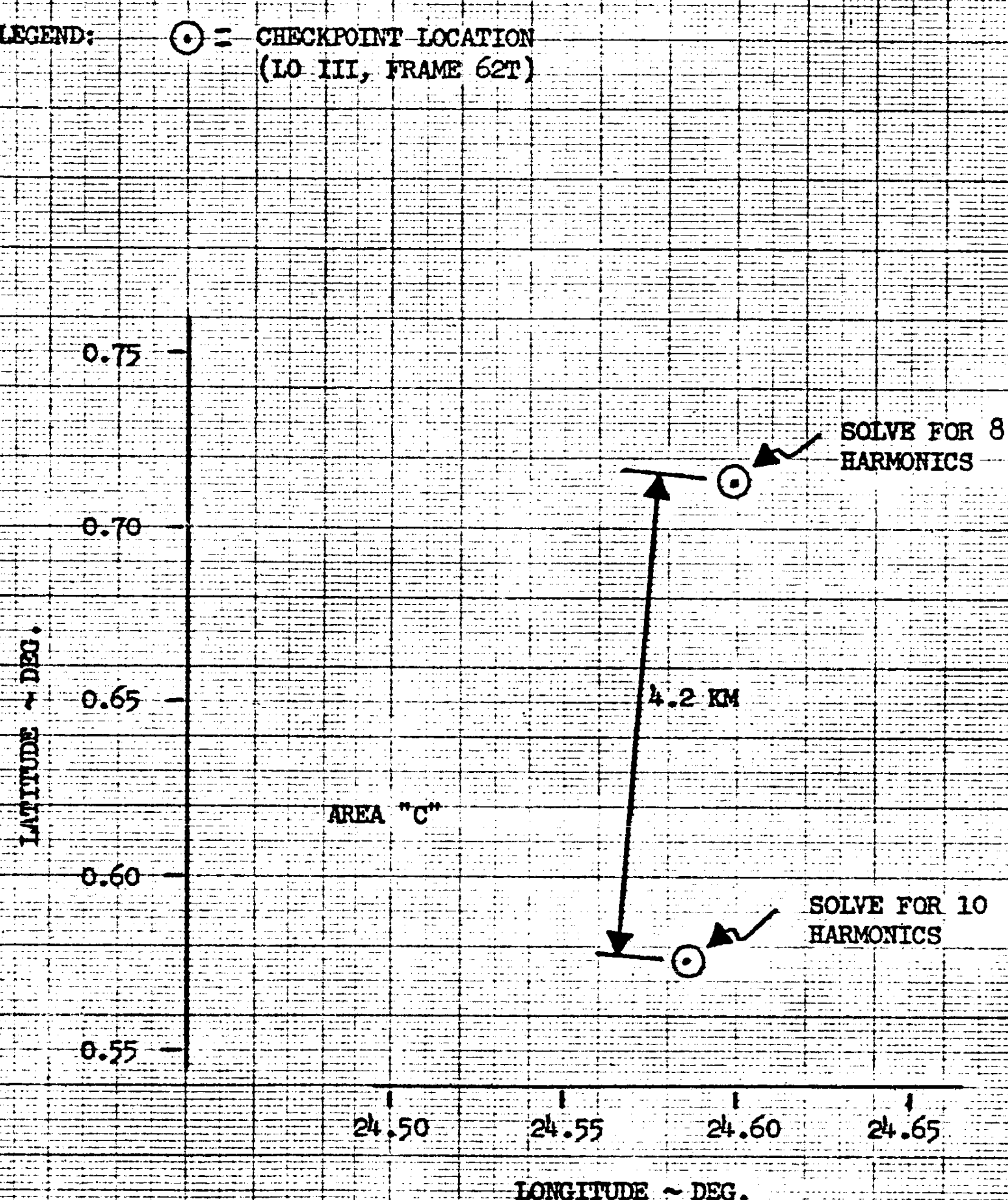

	INITIALS	DATE	REV BY INITIAL	DATE	TITLE	MODEL
CALC					EFFECT OF PROCEDURES ON OD SOLUTIONS	FIGURE 13
CHECK						
APPD.						
APPD.						

U3 4013 8000 REV. 1/66

REV LTR A

STANDARD PROCEDURES INVESTIGATION — SHORT ARC INVESTIGATION

PASS	PASS	DATA ARC	GRAVITATIONAL MODEL LRC 4/17/66	LRC 9/4/66	LRC 7/28b	LRC 7/28a	TBC S-5	LRC 10/24/66	SPHER.	LRC 11/11/66	LRC 10/4/67	LRC 9/30/66	MODIF. 7/28b	AREA, MISSION	DATA ARC	PRIOR ARC METHOD	EPOCH	DOPPLER BIAS SOL'N	GRAV. MODEL LRC 7/28b	TBC S-5
D	III P-7b	4 hours	✓	✓	✓	✓	✓	✓	✓+	X		✓		D, III	75 min.	I	Nom.	No		✓
	"	6	✓	✓+	✓	✓	✓	✓	✓+	X	✓	✓+		"	75	II	Nom.	No		✓
	"	10	✓		✓	✓	✓	✓	✓	✓	✓		✓	"	90	II	Nom.	No		✓
	II P-8a	10	✓		✓	✓	✓	✓	✓	✓	✓+	✓	✓	D, II	90	II	Nom.	No		✓
	"	12	✓		✓	✓	✓	✓	✓	✓	✓+									
	"	15	✓		✓	✓	✓		✓	✓	X									
	V 27a	4	✓		✓	✓	✓	✓	✓	✓	✓	✓		D, V	60	**	Nom.	No	✓	
	"	6	✓		✓	✓	✓	✓	✓	✓	✓	✓		"	60	**	Nom.+10m.	No	✓	
	"	10	✓		✓	✓	✓		✓	✓	✓	✓	✓	"	60	**	Nom.	Yes	✓	
	V 27b	4	✓		✓	✓	✓		✓	✓	✓			"	60	**	Nom.	No		✓
	"	6	X		✓	✓	✓		✓	✓	✓			"	60	**	Nom.+10m.	No		✓
	"	10	✓ -		✓	✓	✓		✓	✓	✓			"	60	**	Nom.	Yes		✓
B	III P-1	6			✓		✓		✓											
	"	6 *			✓		✓		✓											
	V 11a	10			✓		✓		✓											
C	III P-5b	10			✓		✓							C, III	60	II	Nom.	No	✓	
	II P-6b	10			✓		✓													
														C, V	60	**	Nom.	No	✓	
H	III P-11	10			✓		✓													
	V-42a	10			✓		✓													
F	III P-10	10			✓		✓													
	II P-13a	10			✓		✓													

* Perilune data excluded.

** No prior arc = 2-station view.

CONVERGENCE INDICATORS:
- ✓ Converged
- \- Very slow
- ✓+ May have converged (incomplete)
- X Did not converge

	INITIALS	DATE	REV BY INITIALS	DATE	TITLE	MODEL
CALC.					DATA SUMMARY	FIGURE
CHECK					OD PROCEDURES INVESTIGATION	14
APPD						
APPD						

REV LTR A

U3 4011 2000 REV. 2/65

BOEING NO. D2-100814-1

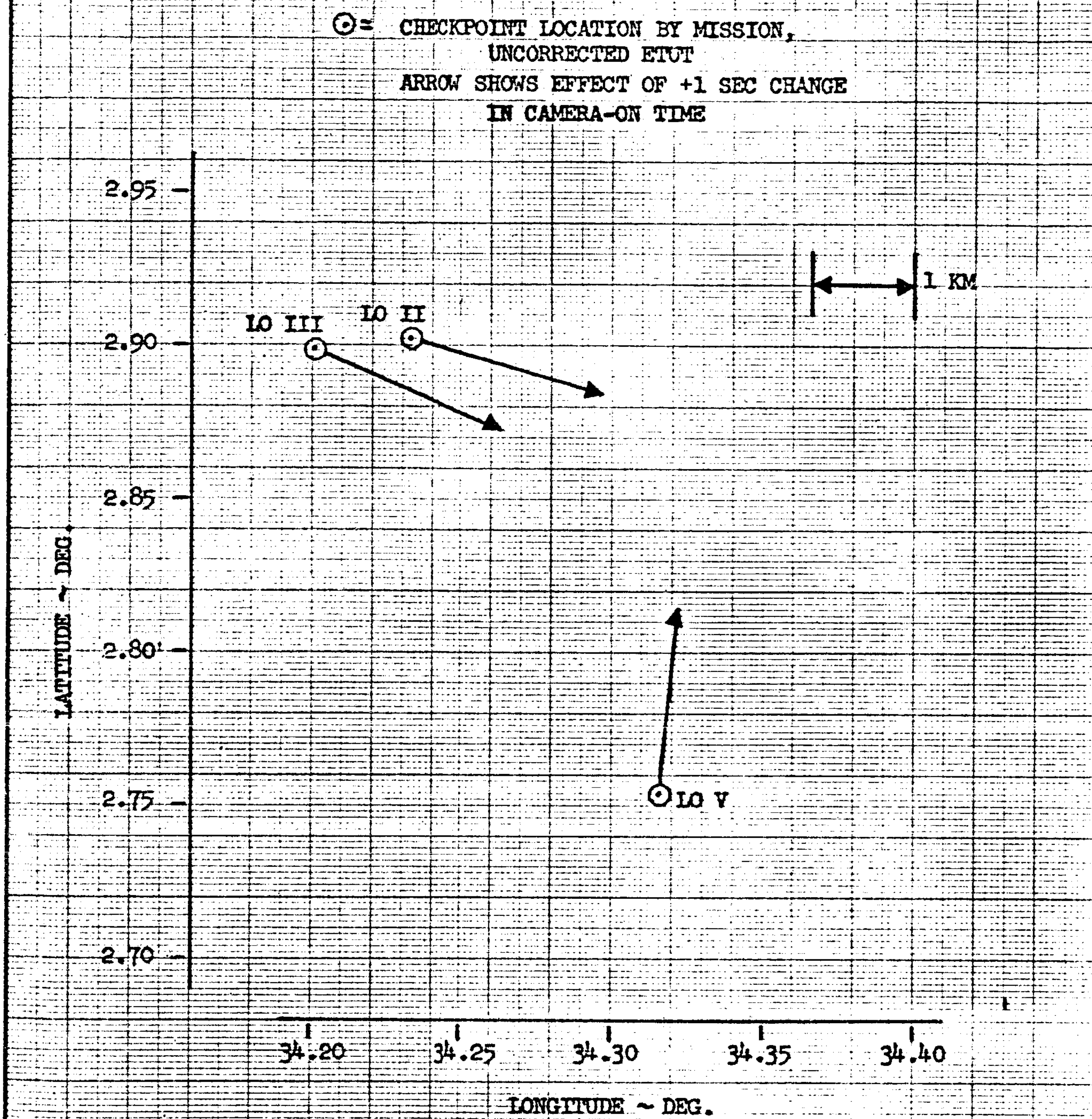

	INITIALS	DATE	REV BY INITIAL	DATE	TITLE	MODEL
CALC					TYPICAL CHECKPOINT PATTERN BEFORE ETUT CORRECTION	FIGURE 15
CHECK						
APPD.						
APPD.						

U3 4013 8000 REV. 1/66

KALMAN FILTER OPTIONS AVAILABLE IN ODPL

OPTION	EPOCH	RESIDUAL FEEDBACK	
1	FLOATING	WITH	AFFECTS ESTIMATE OF
2	FIXED	WITH	STATE VECTOR
3	FLOATING	WITHOUT	AND STATISTICS.
4	FIXED	WITHOUT	
5	FLOATING	WITHOUT	
6	FIXED	WITHOUT	AFFECT ESTIMATE OF
7	FLOATING	WITH	STATISTICS ONLY.
8	FIXED	WITH	
0	STANDARD ODPL LEAST SQUARES FIT		

TYPICAL SEQUENCE OF OPTIONS CHECKED

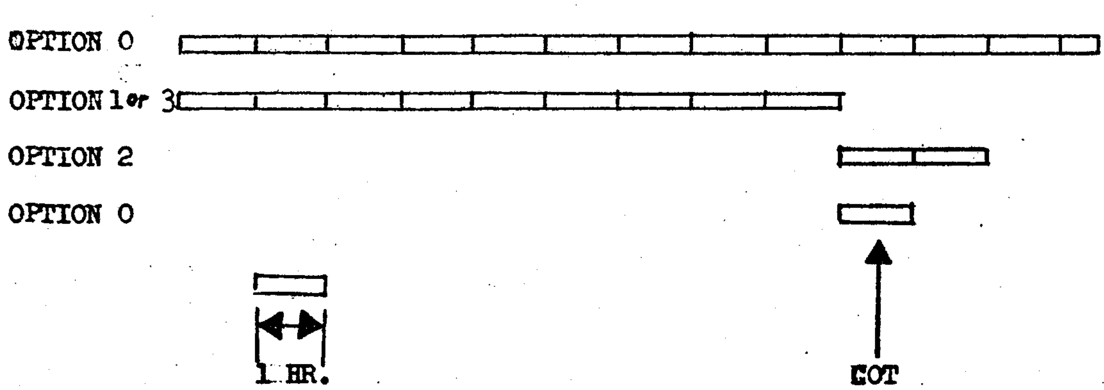

FIGURE 16

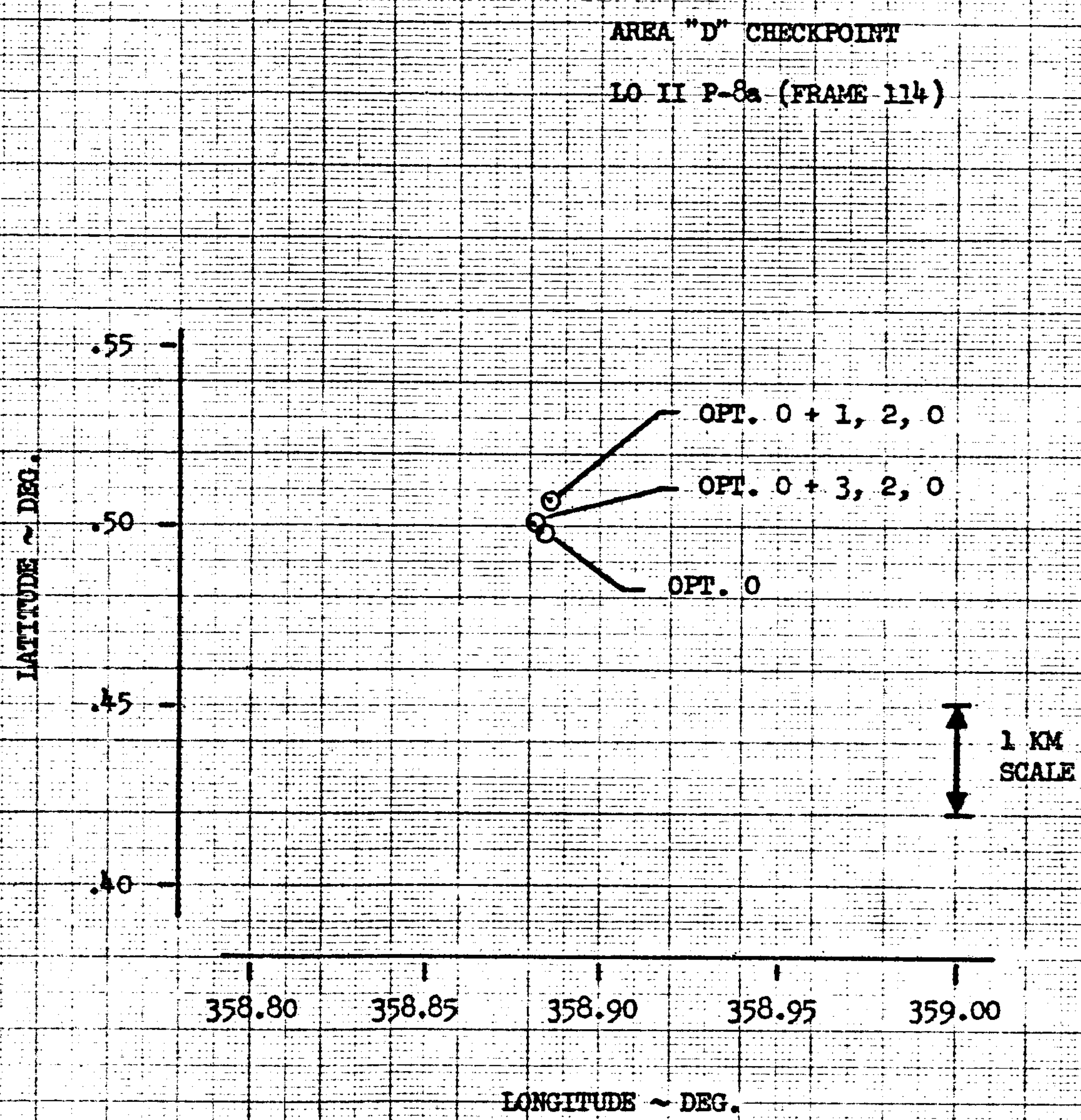

	INITIALS	DATE	REV BY INITIAL	DATE	TITLE	MODEL
CALC	TN	6/66			TWO DIFFERENT FILTER OPTIONS	FIGURE 17
CHECK						
APPD.						
APPD.						

U3 4013 8000 REV. 1/66

REV LTR A

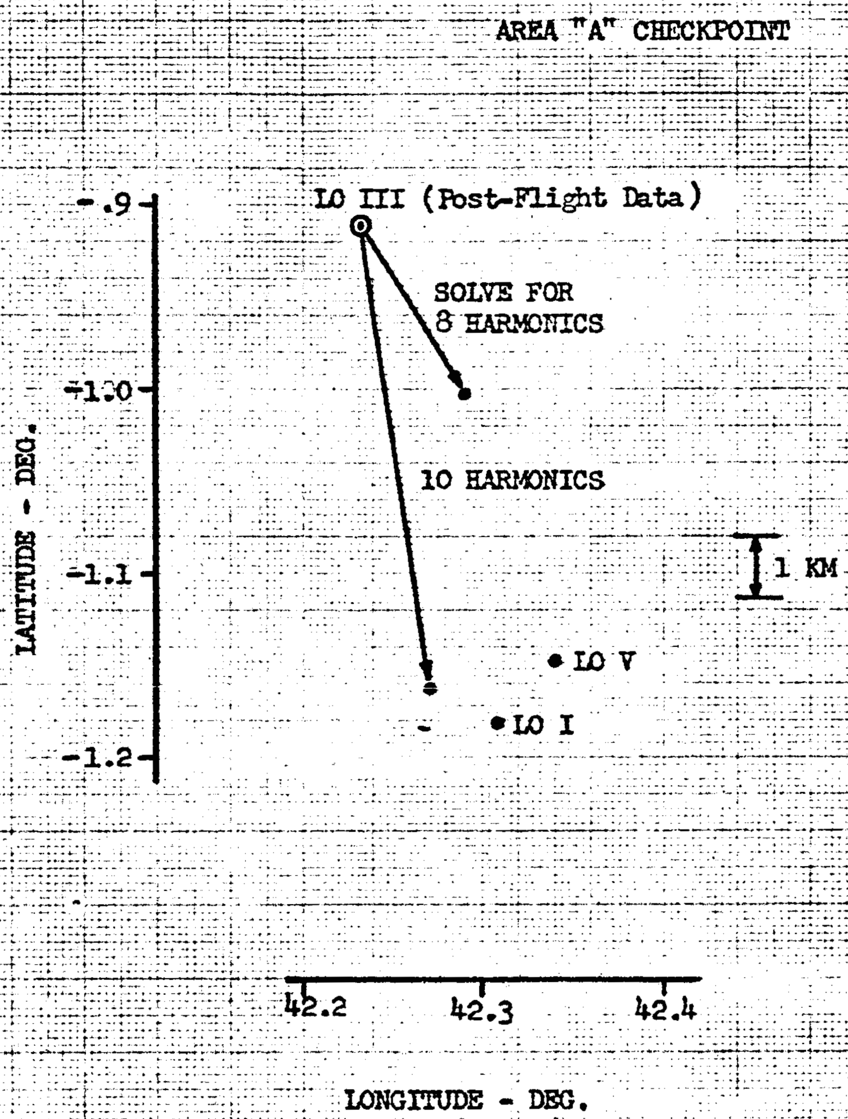

	INITIALS	DATE	REV BY INITIAL	DATE	TITLE	MODEL
CALC					SOLUTION FOR HARMONICS	FIGURE 18
CHECK						
APPD.						
APPD.						

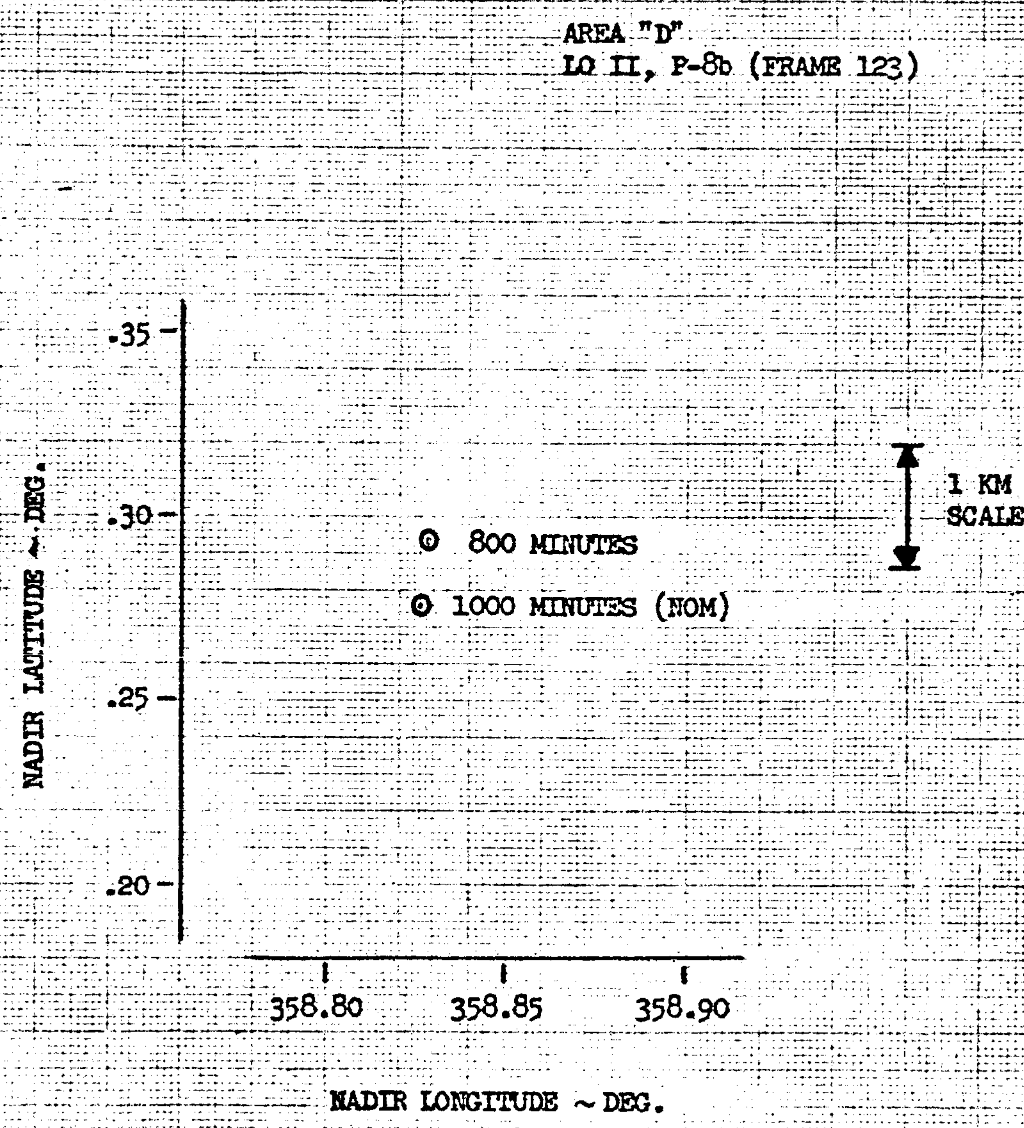

	INITIALS	DATE	REV BY INITIAL	DATE	TITLE	MODEL
CALC					EFFECT OF DATA ARC LENGTH	FIGURE 19
CHECK						
APPD.						
APPD.						

U3 4013 8000 REV. 1/66

REV LTR A

IMPROVED OD PROCEDURES

- LUNAR MODEL, SOLVE FOR LIST
  - LO I, II, III (LOW INCLINATION) - LRC 11/11, SOLVE FOR 10 HARMONICS
  - LO IV } (HIGH INCLINATION) - LRC 7/28 B, UNMODIFIED
  - LO V } (HIGH INCLINATION) - LRC 7/28 B, SOLVE FOR 10 HARMONICS
- PERILUNE DATA - ALL MISSIONS - ALL INCLUDED
- DATA ARC LENGTH - ALL MISSIONS
  - SAME AS FLIGHT PROCEDURES - APPROXIMATELY 12 HOURS
- TRUE ANOMALY AT EPOCH, ALL MISSIONS
  - SAME AS FLIGHT PROCEDURES - APPROXIMATELY ± 150°
- STATE VECTOR FORWARDING (WITHIN ARC), ALL MISSIONS
  - USE SAME HARMONICS AS IN SOLUTION

BOEING

31

FIGURE 20

IMPROVED OD PROCEDURES

ORIGINATOR: NASA LANGLEY RESEARCH CENTER

TITLE: LRC 11/11/66

DATA USED: LUNAR ORBITER I

J20 = 2.07E-4

J30 = -0.446E-4

J40 = -0.209E-4

C21 = 0.088E-4	S21 = -0.411E-4
C31 = 0.435E-4	S31 = 0.107E-4
C41 = -0.051E-4	S41 = -0.102E-4
C22 = 0.276E-4	S22 = -0.058E-4
C32 = -0.052E-4	S32 = 0.0187E-4
C42 = 0.028E-4	S42 = -0.083E-4
C33 = 0.0091 E-4	S33 = -0.033E-4
C43 = -0.0047E-4	S43 = -0.026E-4
C44 = 0.00094E-4	S44 = 0.0017E-4

FIGURE 21

ORIGINATOR: NASA LANGLEY RESEARCH CENTER

TITLE: LRC 7/28B

DATA USED: LUNAR ORBITER IV AND V

KM = 4902.58
J20 = .2092E-3
J30 = -.1738E-4
J40 = -.3793E-4
J50 = .3176E-4
J60 = 0
J70 = 0

C21 = -.1571E-6	S21 = -.5515E-5
C31 = .2272E-4	S31 = -.1355E-4
C41 = -.3263E-5	S41 = .6798E-5
C51 = -.7216E-5	S51 = -.6547E-6
C61 = .5216E-5	S61 = .2231E-5
C71 = .1305E-4	S71 = .3413E-5
C22 = .1766E-4	S22 = -.1667E-5
C32 = .7405E-5	S32 = .2090E-5
C42 = .9158E-7	S42 = -.7879E-6
C52 = .4039E-5	S52 = .1951E-5
C62 = -.1715E-5	S62 = .5328E-6
C72 = -.2053E-5	S72 = -.9328E-6
C33 = ..3755E-5	S33 = .3523E-6
C43 = -.4107E-6	S43 = -.9379E-6
C53 = -.2503E-6	S53 = .9193E-6
C63 = -.5840E-6	S63 = -.1616E-6
C73 = .1342E-6	S73 = -.2469E-6
C44 = -.4731E-7	S44 = .1580E-7
C54 = .1076E-6	S54 = .9155E-7
C64 = .9962E-7	S64 = -.1047E-6
C74 = .5499E-7	S74 = -.1402E-7
C55 = -.4162E-7	S55 = .4836E-7
C65 = -.3961E-8	S65 = -.2166E-7
C75 = -.6878E-8	S75 = .6343E-9
C66 = .4314E-8	S66 = -.6016E-8
C76 = -.1945E-9	S76 = .5396E-9
C77 = -.2571E-9	S77 = .3969E-9

FIGURE 22

USE FOR DRAWING AND HANDPRINTING — NO TYPEWRITTEN MATERIAL

LUNAR RADIUS

EFFECT ON CHECKPOINT LOCATION

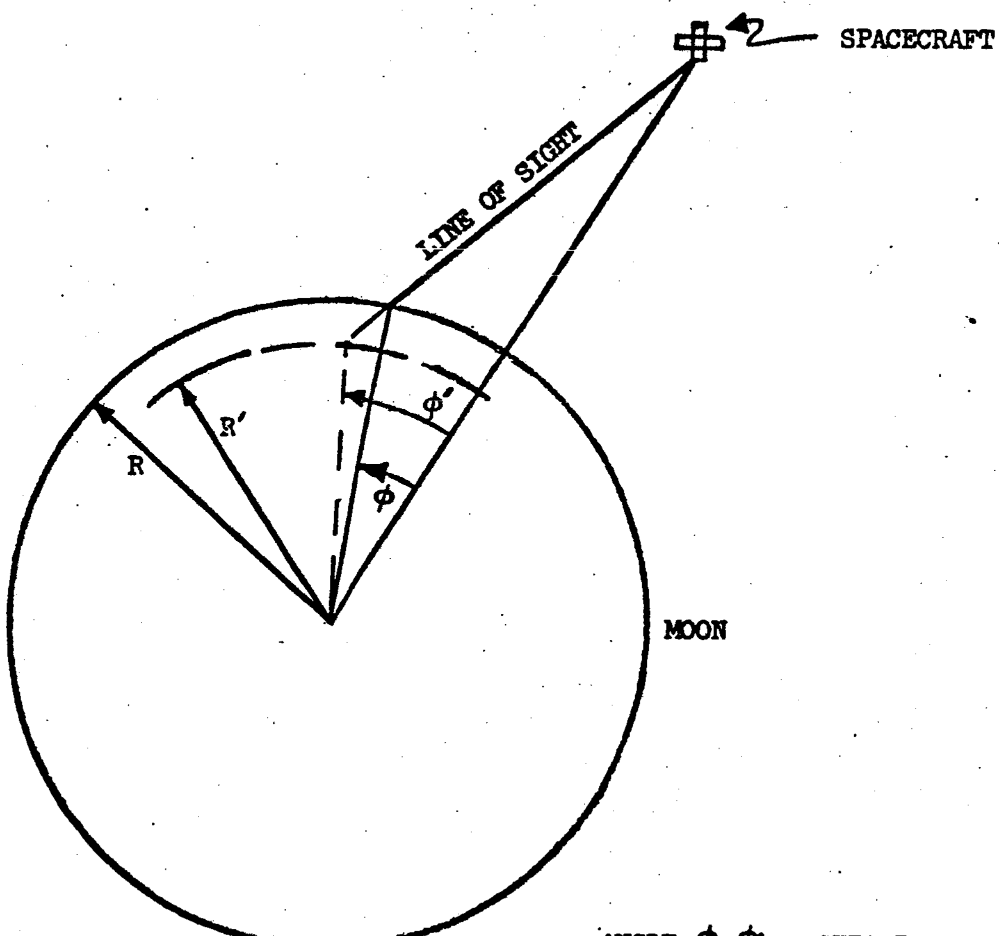

ANGLE φ, φ' = CHECKPOINT LOCATION

FIGURE 23

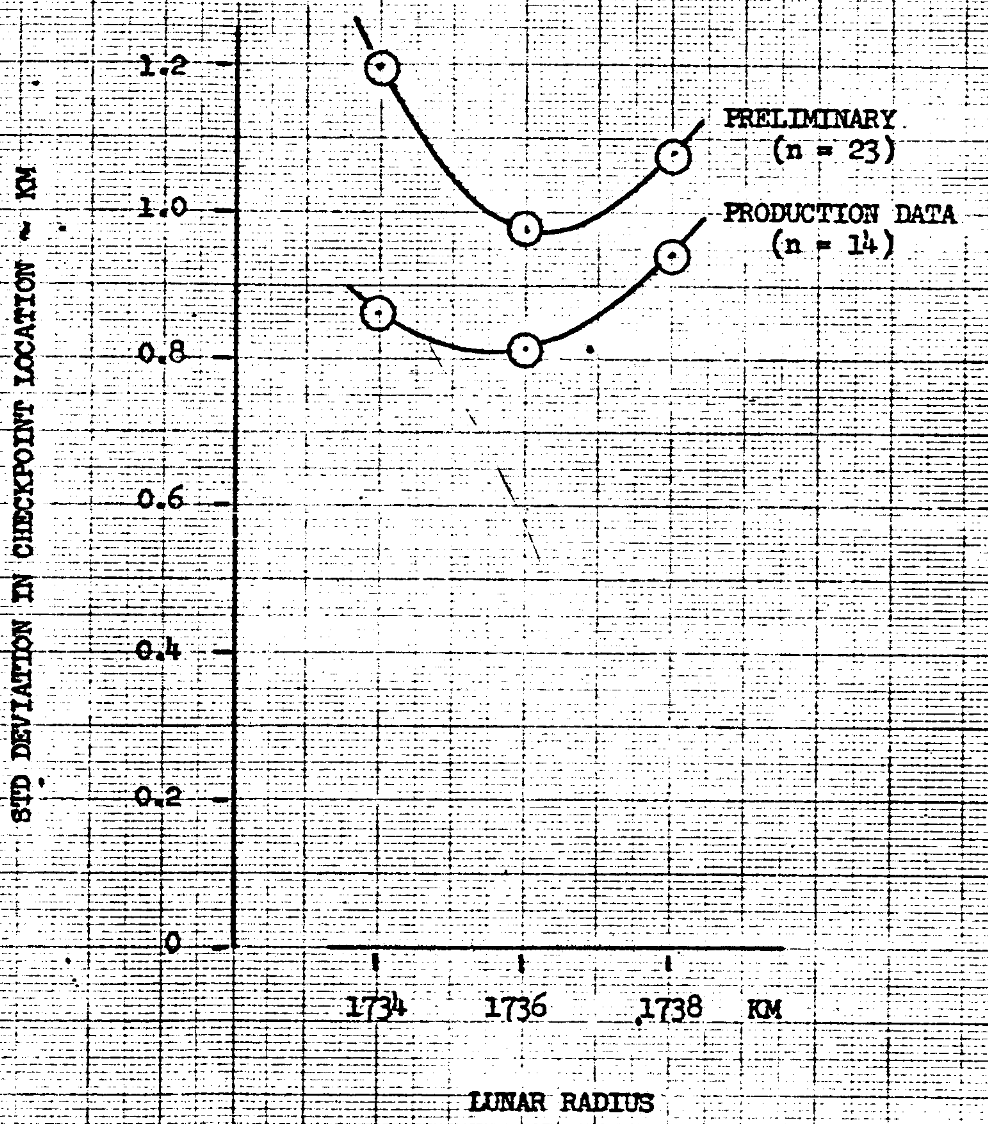

	INITIALS	DATE	REV BY INITIAL	DATE	TITLE	MODEL
CALC	WM 4/68				EFFECT OF LUNAR RADIUS ON CONSISTENCY	FIGURE 24
CHECK						
APPD.						
APPD.						

U3 4013 8000 REV. 1/66

REV LTR A

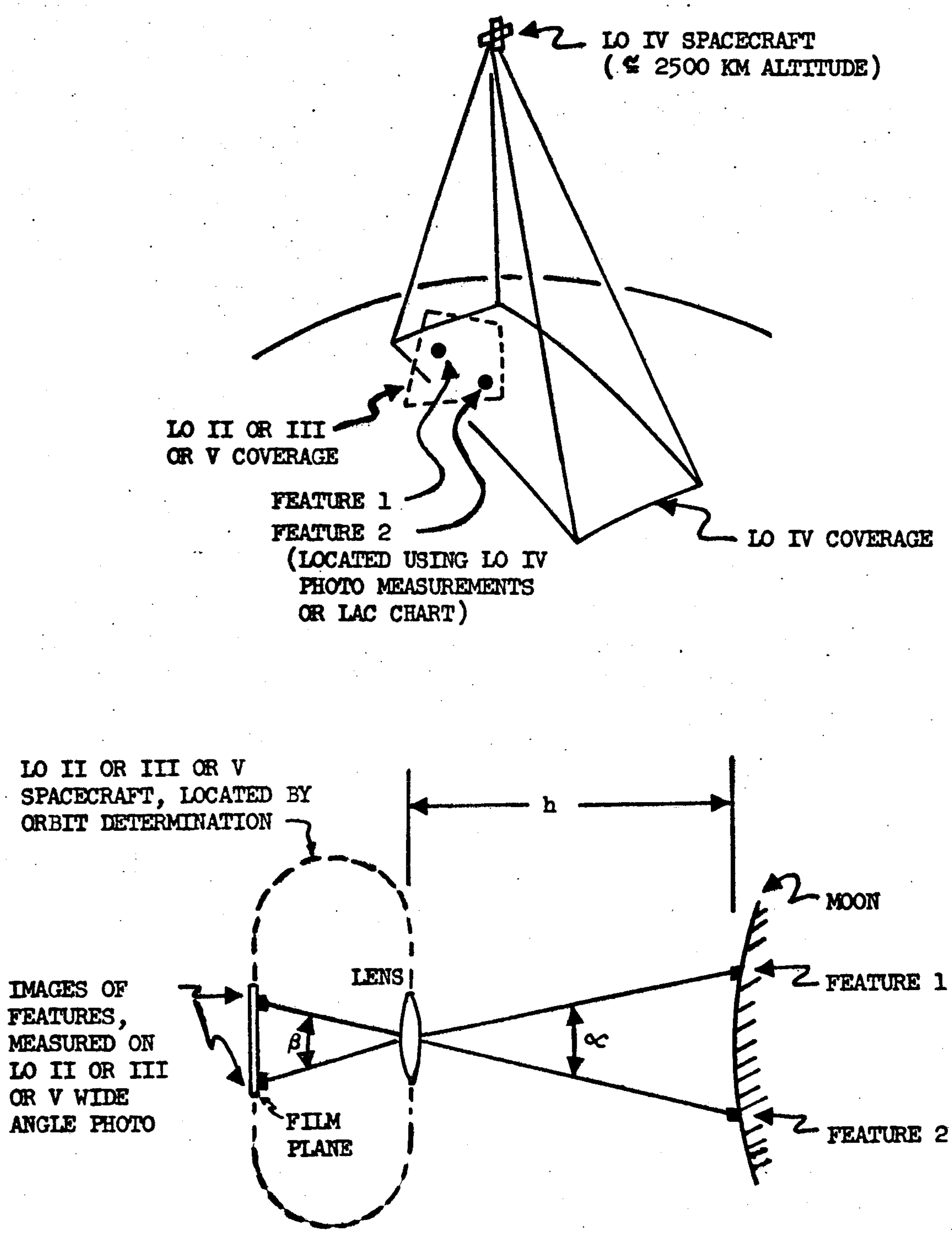

VALUE OF h IS FOUND TO MINIMIZE $\alpha - \beta$

SITE ELEVATION GEOMETRY

FIGURE 25

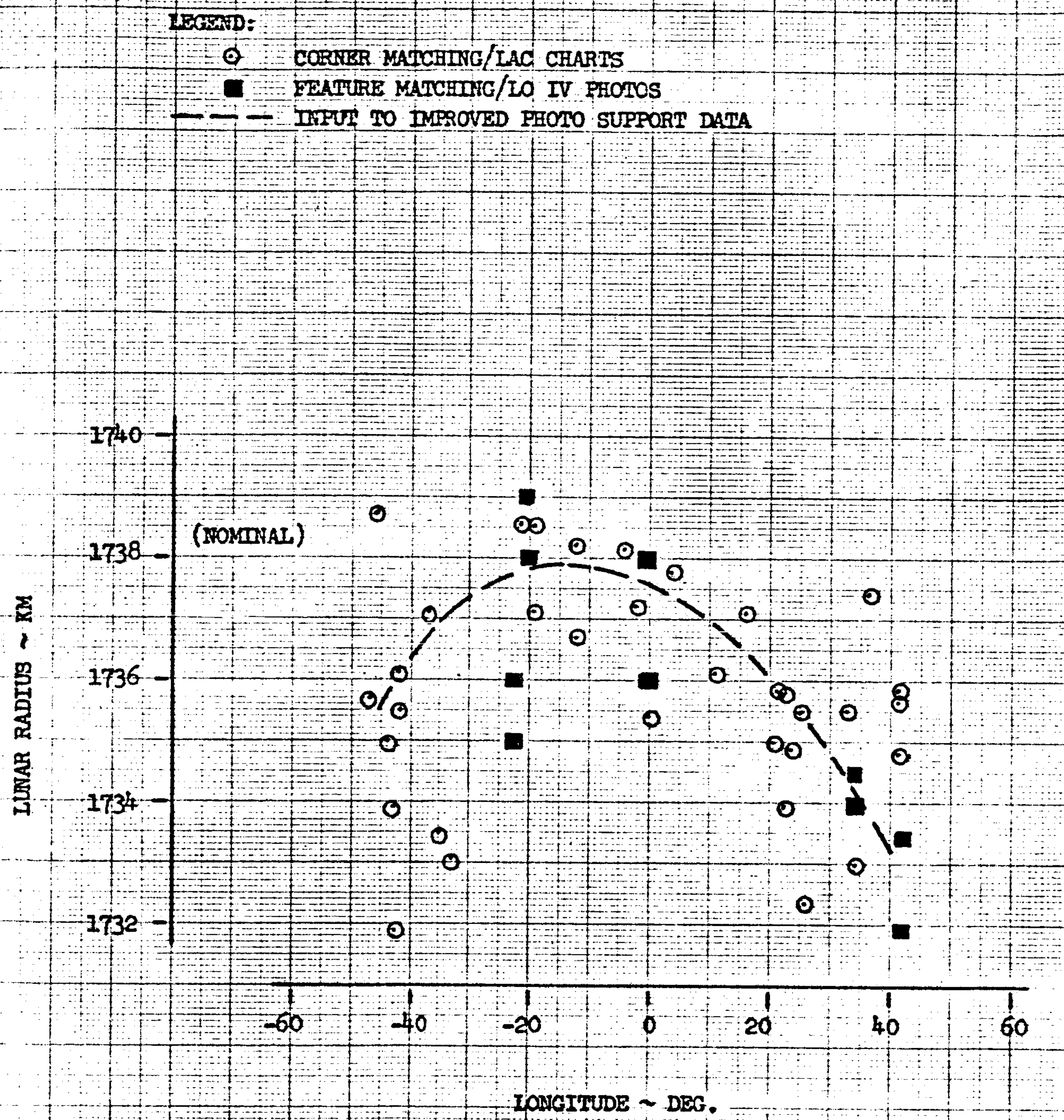

	INITIALS	DATE	REV BY INITIAL	DATE	TITLE	MODEL
CALC					LOCAL LUNAR RADIUS	FIGURE 26
CHECK						
APPD.						
APPD.						

U3 4013 8000 REV. 1/66

REV LTR A

Error Analysis Summary Table

One Sigma Surface Location, Kilometers

Mission	Frame	Note	Spacecraft Altitude (KM)	Camera Axis Tilt ∠ (DEG)	Telephoto Lens		Wide-Angle Lens	
					σ_{LAT} (KM)	σ_{LONG} (KM)	σ_{LAT} (KM)	σ_{LONG} (KM)
I	42		261.2	16.5	.113-.940	.595-.677	.680-2.31	.569-1.11
	116	Large attitude maneuver	1454	4.9	3.95-7.42	.293-3.40	6.26-44.3	3.05-47.3
	137	Apollo Site	52.5	43.0	.185-.310	.435-.590	.132-.956	.306-1.34
	154	Typical of Apollo errors	49.2	5.0	.178-.224	.114-.131	.143-.405	.121-.238
	175	Apollo Site	48.5	19.4	.190-.325	.150-.169	.152-.533	.152-.375
II	22	Typical of Apollo errors	46.0	3.5	.203-.240	.107-.133	.171-.379	.109-.278
	134	Large attitude maneuver	1450	16.6	6.87-15.9	3.66-5.20	6.60-14.1	3.85-8.45
	162		45.8	69.5	1.02-2.58	.214-.317	.545-3.21	.228-1.24
III	37		393	5.1	1.09-1.16	3.72-4.14	1.16-2.22	4.20-6.64
	39		50.1	66.9	.212-4.44	.781-12.7	.143-.488	.391-1.60
	41		57.5	17.0	.184-.573	.157-.190	.0990-.633	.169-.379
	69	Typical of Apollo errors	47.6	7.0	.160-.193	.102-.122	.136-.382	.110-.260
	121	Large attitude maneuver	1461	12.6	6.60-11.6	3.08-4.65	7.40-10.6	3.30-6.43
	140	Apollo Site	46.4	37.6	.231-1.14	.607-3.45	.129-.519	.323-2.30
IV	6	One attitude maneuver	3508	2.7	8.80-16.4	9.03-177.	14.2-17.5	22.0-28.5
	14	Three attitude maneuvers	2746	0.3	16.8-22.2	10.4-14.5	16.3-179.	10.8-125.
	22	Five attitude maneuvers	2979	1.5	21.1-31.8	14.4-50.3	28.9-47.0	22.6-57.0
	75	Large attitude maneuver	6125	0.3	24.0-49.1	13.1-32.4	26.9	13.5
V	21	Large attitude maneuver	3343	17.0	3.57-30.1	15.2-80.0	5.55-19.2	18.4-80.3
	22	Large attitude maneuver	5107	10.1	3.92-34.2	23.5-113.	4.50-14.8	23.7-29.2
	32	Large attitude maneuver	1395	21.0	1.28-1.97	7.09-9.80	1.24-5.90	5.28-26.8
	38	Apollo Site; Large att.man.	98.0	59.2	.432-2.25	2.96-34.4	.407-2.64	1.92-7.24
	63	Large attitude maneuver	95.9	29.3	.351-.435	.293-.580	.344-.623	.202-1.34
	102	Large attitude maneuver	247.8	34.1	1.20-4.10	4.10-6.93	.740-26.6	2.56-35.5
	109	Apollo Site (Typical Apollo errors); Large att.man.	97.3	10.1	.248-.344	.240-.332	.232-.541	.222-.552
	130	Large attitude maneuver	233.5	7.1	.495-.760	.776-.945	.461-1.21	.824-1.59

FIGURE 27

USE FOR DRAWING AND HANDPRINTING — NO TYPEWRITTEN MATERIAL

USE FOR TYPEWRITTEN MATERIAL ONLY

DISTRIBUTION LIST

NAS1-7954

	Copies each
NASA Langley Research Center Langley Station Hampton, Virginia 23365	
Attention: Research Program Records Unit, Mail Stop 122	1
Raymond L. Zavasky, Mail Stop 117	1
Wilbur L. Mayo, Mail Stop 159	1
I. G. Recant, Mail Stop 159	1
William H. Michael, Jr., Mail Stop 152A	1
Albert A. Schy, Mail Stop 152B	1
NASA Ames Research Center Moffett Field, California 94035 Attention: Library, Stop 202-3	1
NASA Flight Research Center P.O. Box 273 Edwards, California 93523	1
Jet Propulsion Laboratory 4800 Oak Grove Drive Pasadena, California 91103 Attention: Library, Mail 111-113	1
NASA Manned Spacecraft Center 2101 Webster Seabrook Road Houston, Texas 77058 Attention: Library, Code BM6	1
NASA Marshall Space Flight Center Huntsville, Alabama 35812 Attention: Library	1
NASA Wallops Station Wallops Island, Virginia 23337 Attention: Library	1
NASA Electronics Research Center 575 Technology Square Cambridge, Massachusetts 02139 Attention: Library	1
NASA Lewis Research Center 21000 Brookpark Road Cleveland, Ohio 44135 Attention: Library, Mail Stop 60-3	1

USE FOR TYPEWRITTEN MATERIAL ONLY

DISTRIBUTION LIST

NAS1-7954

	Copies each
NASA Goddard Space Flight Center Greenbelt, Maryland 20771 Attention: Library	1
NASA John F. Kennedy Space Center Kennedy Space Center, Florida 32899 Attention: Library, Code IS-CAS-42B	1
National Aeronautics and Space Administration Washington, D. C. 20546 Attention: Library, Code USS-10	1
L. Kosofsky, Code MAL	1
NASA Manned Spacecraft Center 2101 Webster Seabrook Raod Houston, Texas 77058 Attention: J. Sasser, Code TH3	3
W. R. Wollenhaupt, Code FM4	1
Army Map Service 6500 Brooks Lane Washington, D. C. 20315 Attention: D. Light, Code 12440	1
C. MacAfoos, Code 11910	1
Aeronautical Chart and Information Center 2nd and Arsenal Street St. Louis, Missouri 63118 Attention: C. F. Martin, ACDEG-2	1
R. Carder, ACO	1
National Space Science Data Cenyer Goddard Space Flight Center Greenbelt, Maryland 20771 Attention: K. Michlovitz, Code 601	50 plus reproducibles
Bellcomm, Inc. 995 L'Enfant Plaza North S.W. Washington, D. C. 20024 Attention: D. B. James	1
U. S. Geological Survey 345 Middlefield Road Menlo Park, California 94025 Attention: H. Masursky	2

DISTRIBUTION LIST

NASl-7954

	Copies each
Dr. Donald Wise Department Department of Geology Franklin Marshall College Lancaster, Pennsylvania 17604	1
University of Arizona Tucson, Arizona 85721 Attention: Dr. G. P. Kuiper	1
Professor E. A. Whitaker	1
University of California P. O. Box 109 LaJolla, California 92037 Attention: Dr. H. C. Urey	1
NASA Scientific and Technical Information Facility P. O. Box 33 College Park, Maryland 20740	17

USE FOR TYPEWRITTEN MATERIAL ONLY